Thermophysical Properties of Thoria-based Fuels

T. R. Govindan Kutty, Joydipta Banerjee and Arun Kumar

Abstract The behavior of nuclear fuel during irradiation is largely dependent on its thermophysical properties and their change with temperature and burnup. Experimental data on out-of-pile properties such as melting point, density, thermal conductivity, and thermal expansion are required for fuel design, performance modeling, and safety analysis. The variables that influence the out-of-pile properties are fuel composition, temperature, porosity, microstructure, and burnup. Among the above-mentioned properties, thermal conductivity of nuclear fuel is the most important property which influences almost all the processes such as swelling, grain growth, and fission gas release, and limits the linear power. The changes in thermal conductivity occur during irradiation by the formation of fission gas bubbles, porosities, build-up of fission products, and by the change of fuel stoichiometry. Melting point plays a crucial role in determining the power to melt the fuel and decides the operating linear heat rating. The coefficient of thermal expansion (CTE) is needed to calculate stresses occurring in the fuel and cladding on change in temperature. In safety analysis, the values of thermal expansion data are required in determining the gap conductance and the stored energy.

1 Introduction

The behavior of nuclear fuel during irradiation is largely dependent on its physicochemical properties and their change with temperature and burnup [1]. Thermal conductivity is an important parameter to understand the performance of the fuel

T. R. Govindan Kutty (✉)
Formerly at Radiometallurgy Division, Bhabha Atomic Research Centre,
Mumbai 400085, India
e-mail: trgovindankutty@gmail.com

J. Banerjee · Arun Kumar
Radiometallurgy Division, Nuclear Fuels Group, Bhabha Atomic Research Centre,
Mumbai 400085, India

D. Das and S. R. Bharadwaj (eds.), *Thoria-based Nuclear Fuels*,
Green Energy and Technology, DOI: 10.1007/978-1-4471-5589-8_2,

pins under irradiation [2]. It is highly dependent on physical structure, state, chemical composition, and is one of the most important properties for predicting fuel and material performance [3]. If the thermal conductivity is low, the temperature gradient in the radial direction of the fuel pellet is large which results in high temperature at the central part of the fuel pin [2, 3]. The thermal conductivity of nuclear fuel influences almost all important processes such as fission gas release, swelling, grain growth etc. and limits the linear power [4, 5]. The changes in thermal conductivity occur during irradiation by the formation of fission gas bubbles, build-up of fission products, and by the change of oxygen-to-metal ratio (O/M) [6]. Hence, the knowledge of thermal conductivity is needed to evaluate the performance of nuclear fuels. The coefficient of thermal expansion (CTE) values is needed to calculate stresses occurring in the fuel and cladding. If the thermal expansion varies considerably between the fuel and cladding, then stresses will be accumulated during the thermal cycling [7]. This can lead to deformation of the cladding and eventually may result in the breakage of the cladding. Hence, precise evaluation of CTE data of the fuel is needed.

Other important thermophysical properties to be considered are melting point and density. Thorium and uranium oxide fuels used in nuclear reactors have very high melting points, but low density and they suffer from poor thermal conductivity, because in these insulating oxides only phonons (lattice vibrations) conduct heat. Understanding the physics underlying transport phenomena due to electrons and lattice vibrations in actinide systems is an important step toward the design of better fuels [8].

Thermophysical properties of materials depend on various factors, such as microstructure, porosity and its distribution, thermal treatment employed, production technology used, radiation exposure undergone, and other unidentified factors leaving aside the temperature effect [1]. Improving the technology for nuclear reactors through better computer codes and more accurate data of materials property, which can contribute to improved performance as well as economics of future plants by getting rid of currently used large design margins. Accurate representations of thermophysical properties under relevant temperature and neutron fluence conditions are therefore, necessary for evaluating reactor performance under normal operation and accidental conditions [2].

Prior to deploying new fuels and structural materials in a nuclear reactor, its thermophysical properties must be known. The fuel temperature is determined by the thermal conductivity. Such properties of the fuel are not constant during the irradiation period in the reactor, but change with the burnup. Therefore, the evaluation of the thermophysical properties of fuel, including a reliable uncertainty assessment, is required by the nuclear reactor design [3]. A high confidence level on the fuel performance can only be reached from a good interpretation of the irradiation data followed by post-irradiation examinations. A prerequisite for this is to have data on out-of-pile properties such as thermal conductivity or thermal diffusion that allows to understand the influence of parameters such as temperature, temperature gradient, stress, stress gradient, fission rate, and impurities that

are effective during the operation. Safety analyses are required by regulatory authorities to prove that the fuel can be burned safely in the reactors. These safety analyses require calculations with safety codes that need the appropriate thermophysical properties of the fuel. These important informations are used by thermohydraulic codes to define operational aspects and to assure the safety, when analyzing various potential accidental scenarios. For each property, the variables that influence the property are to be described, followed by a review of the available data and correlations. Variables considered are temperature, composition, porosity (p), burnup (B), and oxygen-to-metal (O/M) ratio [9, 10].

Due to its higher thermal conductivity, during normal operation, ThO_2-based fuel will operate with somewhat lower fuel temperatures and release less fission gas than UO_2 fuel at corresponding powers and burnups. This will allow for higher prepressurization and thereby minimizes cladding creep down and fuel cladding mechanical interactions at high burnup and thereby possibly allow for higher burnup use of this material. During an accident such as a large loss-of-coolant accident (LOCA), ThO_2–UO_2 fuel will have less stored energy but a slightly higher internal heat generation rate than UO_2 fuel at similar power levels [11]. As a result, certain parameters for accident evaluation such as the maximum cladding temperature and the timing of fuel rod rupture are expected to be slightly different [8]. These expected differences in behavior between ThO_2–UO_2 fuel rods and UO_2 fuel rods need to be quantified for an objective evaluation of the performance of ThO_2–UO_2 fuel. The mixed ThO_2–UO_2 fuel reduces the amount of total plutonium production by a factor of 3.2 and the ^{239}Pu production by a factor of about 4, when compared with conventional UO_2 fuel irradiated to 45 GWD/t [9]. The plutonium that is produced in the mixed ThO_2–UO_2 fuel is high in ^{238}Pu, producing copious amounts of decay heat and spontaneous neutrons making it proliferation resistant. A mixture of ThO_2 and UO_2 is much more resistant to long-term corrosion in air or oxygenated water than UO_2. Thus, ThO_2–UO_2 is a superior waste form if the spent fuel is slated for direct disposal rather than reprocessing.

2 Melting Point

A very important thermophysical property to be considered for an engineering material, like nuclear fuel, is its melting point. The onset of melting at the centerline of the fuel rod has been widely accepted as an upper limit to the allowable thermal rating of nuclear fuel elements [11, 12]. The melting point must be taken into account when considering a new fuel, as it limits the power that can be extracted from the fuel element. The knowledge of the melting point is also important in the fabrication of chemically homogeneous pellets like thoria–urania since ThO_2 (3,663 K) and UO_2 (3,100 K) have high melting points and relatively low diffusion coefficients at normal sintering temperatures [13].

As a pursuit for the better fuel, it is crucial to understand the underlying transport phenomena due to electrons and lattice vibrations in actinide systems.

According to the Lindemann criterion, solids with large Debye frequencies have high melting points [14]. This is typically found in insulators where atomic bonds are strong due to lack of free electrons. Thorium contains no occupied 5f states while uranium has two unpaired 5f valence electrons, and therefore uranium and thorium possess very different electronic and chemical properties. Since melting point is an important property, it is worth considering from the standpoint of the bonding present in actinide elements [15]. The highest melting points for the actinide metals are for Th and Pa metals. The effect of f-orbitals on the melting point is maximized with Np and Pu; both have very low melting points, which are believed to be a reflection of f-orbital repulsion [16]. Uranium has multiple oxidation states (3+ through 6+) which allow UO_2 to be easily oxidized to U_3O_8 or UO_3, by incorporating interstitial O atoms. In contrast, thorium only exhibits one oxidation state (4+) and hence cannot be oxidized beyond ThO_2 [9, 17]. Among the actinide oxides, only ThO_2 is a white insulating solid and the other AnO_2 solids are all dark and opaque and poorly conducting. While in UO_2 the 5f electrons, which occupy an energy band from 1.37 to 1.50 eV cause a strong visible light absorption resulting in a dark gray color of this oxide. The consequent absence of low electrons in the valence band is the cause of the high transparency of stoichiometric thoria and the low spectral emissivity in the visible range at room temperature [17].

Thorium dioxide exists up to its melting point as a single cubic phase with the fluorite crystal structure, isomorphous, and completely miscible with UO_2. Unlike UO_2, ThO_2 does not dissolve oxygen to a measurable extent. Therefore, it is stable at high temperature in oxidizing atmosphere. On prolonged heating to 1,800–1,900 °C in vacuum, it blackens with loss of oxygen, although the loss is insignificant to be reflected in lattice parameter or in chemical analysis. On reheating in air to 1,200–1,300 °C, the white color is restored.

The melting points of the nuclear fuels are shown to be influenced by the following factors: stoichiometry and composition, irradiation dose, impurities and their contents.

2.1 ThO_2

The melting point of ThO_2 was experimentally measured or estimated by several authors [18–26]. Their results are summarized in Table 1. As it can be seen from the Table, the reported values vary from 3,323 to 3,803 K. Peterson and Curtis [26], in their compilation of data on thorium-based ceramics, arrived at two different values, e.g., 3,573 ± 100 K from the work of Lambertson et al. [21] on ThO_2–UO_2 system and 3,663 K from the work of Benz [22] on Th–ThO_2 system. Lambertson et al. [21] first estimated the melting point of ThO_2 to be between 3,558 and 3,828 K and subsequently arrived at an intermediate value of 3,623 K by extrapolating the melting point data of $(Th,U)O_2$ compositions corresponding to zero UO_2 content. They further refined their data by introducing some corrections

Table 1 Melting point of ThO_2 determined by various authors

Year	Author	Melting point (*K*)
1929	Ruff et al. [18]	3,323
1932	Wartenberg and Reusch [19]	3,803
1953	Geach and Harper [20]	3,323 ± 25
1953	Lambertson et al. [21]	3,573 ± 100
1969	Benz et al. [22]	3,663 ± 100
1970	Christensen [27]	3,543
1972	Chikalle et al. [23], TECDOC-1319	3,573
1975	Rand [25]	3,643 ± 30
1984	Belle and Berman [12]	3,640 ± 30
1992	ITU [25]	3,640 ± 20
1996	Ronchi and Hiernaut [24]	3,651 ± 17

for the liquidus/solidus curve to effect a curvature correction for the pure ThO_2 end to that of pure UO_2 end of the temperature—composition diagram. Their final recommended data was 3,575 K, which is in good agreement with the data 3,543 K recommended by Christensen [27] from his experimentally measured melting point data on ThO_2–UO_2 system and subsequent extrapolation to zero UO_2 content. Rand [25], however, disagrees with the curvature corrections made by others on the thoria or urania rich side of the temperature composition curve. He justified that the curvature need not be same at both the terminal compositions and the difference could be due to the loss of 'O' from UO_2 in urania-rich side, which is different for thoria-rich side. He recommended a value of 3,643 ± 30 K. Belle and Berman [12] used 3,640 K as the melting point of ThO_2, recommended by Rand [25] in his work on ThO_2. Ronchi and Hiernaut [24] had recently measured the melting temperature of ThO_2 (both stoichiometric and hypostoichiometric) material experimentally by heating a spherical sample by four symmetrically spaced pulsed Nd YAG laser and observing the cooling/heating curve with time. For stoichiometric ThO_2, the measured melting point was found to be 3,651 ± 17 K. The data of Ronchi and Hiernaut [24] reasonably agrees with the data generated by Benz [22] (3,660 ± 100 K) and is also close to that recommended by Rand [25] (3,643 ± 30 K). All these values are markedly different from those of Lambertson et al. [21]. It is also well understood that the curvature difference at the uranium- and thorium-rich side of the temperature versus composition diagram is quite justifiable and was attributed to the loss of oxygen. Hence, the recommended melting temperature of ThO_2 should be taken as 3,651 ± 17 K, and is in fairly good agreement with majority of the previous studies. The value measured at the Institute for Transuranium Elements (ITU) (3,640 ± 20) K, is very close to the value reported by Rand [25].

Measurements of the cooling curves of molten ThO_2 and $ThO_{1.98}$ reveal that the stoichiometric compound melts congruently at 3,651 K, while the hypostoichiometric oxide displays a liquidus at 3,628 K and a solidus transition at 3,450 K. Ronchi et al. [24] conducted pulse-heating experiments on thoria and showed that this compound exhibits a premelting transition at 3,090 K whose features are

analogous to those observed in other ionic compounds having fluorite type structures. A class of diatomic compounds which crystallize in the face-centered cubic fluorite lattice (space group Fm3m), and whose component atoms have very different mobilities, exhibit at a temperature corresponding to about 80 % of the absolute melting temperature, a premelting transition. The discovery of this transition in UO_2 [12] gave rise to a number of investigations aimed at defining its nature and possible effects on the high temperature properties of this technologically important material. In ThO_{2-x}, the dependence of the transition temperature, T_c on stoichiometry was found to be weaker than hypostoichiometric urania and exhibits an opposite trend, with T_c decreasing with x.

To conclude, the melting temperature of ThO_2 recommended from this assessment is 3,651 ± 17 K and is in fairly good agreement with majority data available in the literature.

2.2 UO_2

The melting point of UO_2 given in MATPRO [28] is 3,113.15 K. This temperature is based on the measurement made by Brassfield et al. [29] and the equations for the solids and liquids boundaries of the UO_2–PuO_2 phase diagram given by Lyon and Bailey [30]. The recommended values by ORNL [31] for $UO_{2.00}$ are 3,120 ± 30 K and for PuO_2 is 2,701 ± 35 K. This value for UO_2 has been recommended by Rand et al. [32] from their analysis of 14 experimental studies of the melting temperature of UO_2. This recommendation of Rand et al. [32] was accepted internationally and was recommended in the assessment of UO_2 properties by Harding et al. [33] in their 1989 review of material properties for fast reactor safety. The melting point of UO_2, according to Latta et al. [34] is 3,138 ± 15 K, which is considerably higher than that of Christensen (3,073 K) [35]. Belle and Burman [12] recommended the melting temperatures of UO_2 as 3,120 K, with an error of probably ±30 K.

In recent experimental measurements of the heat capacity of liquid UO_2 using laser heating of a UO_2 sphere, Ronchi et al. [36] made several measurements of the freezing temperature of UO_2 on different samples. For specimens in an inert gas atmosphere with up to 0.1 bar of oxygen, they obtained melting points in the interval 3,070 ± 20 K. Higher melting temperatures (3,140 ± 20 K) were obtained for samples in an inert gas atmosphere without oxygen. The variation in melting temperature is in accordance with the expected lower oxygen-to-uranium (O/U) ratio in the latter samples. The melting point of UO_2 drops on variation O/M ratio around stoichiometry: for example, if the melting point of stoichiometric UO_2 is 3,138 K, its value drops to 2,698 K at an O/U ratio of 1.68 and to 2,773 K at an O/U ratio of 2.25. The effect of irradiation is lowering of the melting point of UO_2. At a burnup of 1.5×10^{21} fissions/cm^3, it has been reported [12] that the melting point drops to 2,893 K. Typical values of melting points for UO_2 and PuO_2 obtained by various authors are given in Table 2.

Table 2 Melting point of UO_2 and PuO_2 determined by various authors [31]

	UO_2 (in *K*)	PuO_2 (in *K*)	Remarks
Lyon and Baily [30]	3,113 ± 20	2,663 ± 20	
Aitkens and Evans [146]	3,120 ± 30	2,718 ± 35	
Latta et al. [34]	3,138 ± 15		
Adamson et al. [147]	3,120 ± 30	2,701 ± 35	BU: 0.4 MWD/kg
MATPRO [148]	3,113.15	2,647	BU: 3.2 MWD/kg
Komatsu [149]	3,138 ± 15	2,718	BU: 0.7 MWD/kg
Rand et al. [32]	3,120 ± 30		
Ronchi et al. [36]	3,075 ± 30		
Christensen [37]	3,073		
Belle and Berman [12]	3,120 ± 30		
Belle and Berman [12]	2,893		BU: 1.5×10^{21} fissions/cm^3

BU burnup

2.3 ThO_2–UO_2 System

Phase diagram studies of the ThO_2–UO_2 system have been reported by several authors. Lambertson et al. [21] used a quench technique, Christensen [27, 37] a tungsten filament technique, whereas Latta et al. [34] applied a thermal arrest method. The phase diagram of ThO_2–UO_2 can be constructed with the help of the melting points and enthalpies of fusion of the end members, assuming ideal solid solution behavior in both liquid and solid state. The results of the phase diagram measurements are given in Fig. 1 showing UO_2 and ThO_2 form a continuous series of solid solutions. The measurements of Christensen [27] and Latta et al. [34] show a shallow minimum at 2 and 5 mol% ThO_2, respectively. The melting points calculated for some intermediary composition are shown below in Table 3 [38–49].

There is no direct experimental measurement on the heat of fusion of ThO_2 or ThO_2–UO_2 solid solution. The most probable value is that of Fink for UO_2 as 74.8 ± 1 kJ/mol [50]. The recommended value for ThO_2 is 90.8 kJ/mol [40].

2.4 ThO_2–PuO_2 System

Freshley and Mattys [41, 42] have shown that ThO_2 and PuO_2 form a complete solid solution (Fig. 2) in the whole composition range like ThO_2 and UO_2. A continuous series of solid solution has also been reported by Mulford and Ellinger [44]. They found only a single fluorite structure by X-ray diffraction (XRD) and also showed that the lattice parameter varied linearly with composition.

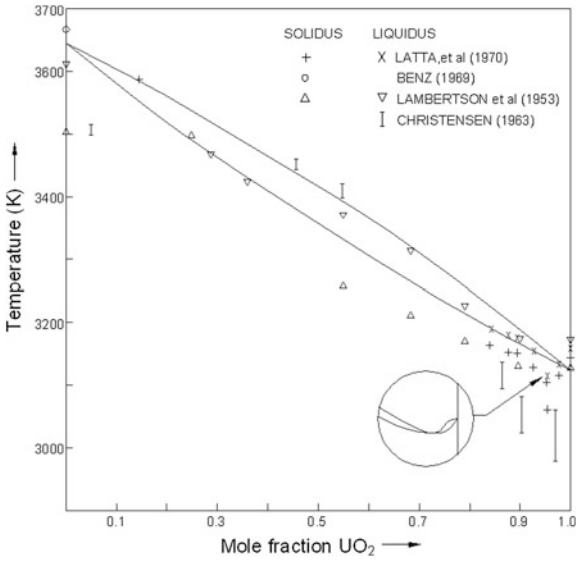

Fig. 1 ThO_2–UO_2 phase system [12]

Table 3 Melting temperatures of ThO_2–UO_2 solid solution [12]

Composition (mol% UO_2)	Solidus temperature (*K*)	Liquidus temperature (*K*)
0	3,640	3,640
10	3,580	3,600
20	3,520	3,550
30	3,460	3,510
40	3,410	3,460
50	3,360	3,410
60	3,310	3,360
70	3,260	3,310
80	3,210	3,250
90	3,160	3,190
100	3,120	3,120

Dawson [45] has made magnetic susceptibility measurements on PuO_2 and ThO_2 mixtures and implied that PuO_2 and ThO_2 form solid solutions which follow the Vegard's law. The lattice parameter of fluorite type cubic phase was found to decrease regularly from 0.5597 nm for ThO_2 to 0.5396 nm for pure PuO_2 [43]. Due to the limited amount of experimental data, a more accurate assessment of the phase diagram is not yet possible. The melting point of the ThO_2–PuO_2 solid solutions, containing various amounts of PuO_2, was measured in helium. The melting point of the specimens containing less than 25 % ThO_2 was found to be unchanged as shown in Fig. 3 [42]. The melting point of a PuO_2 sample (whose purity was not specified) used in their study is 2,533 K, which is 130 K lower than the assessed value of Table 2.

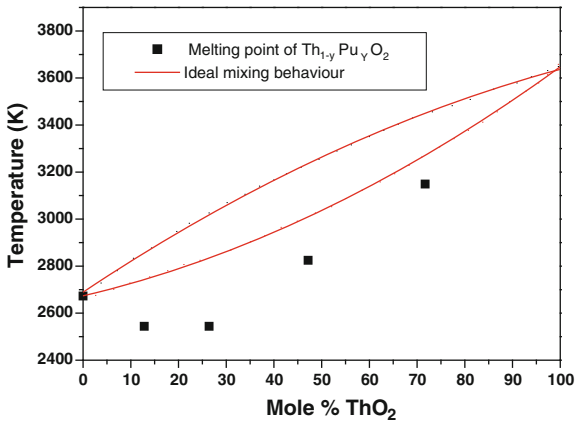

Fig. 2 Phase diagram of ThO_2–PuO_2 system [38]. (permission from Elsevier)

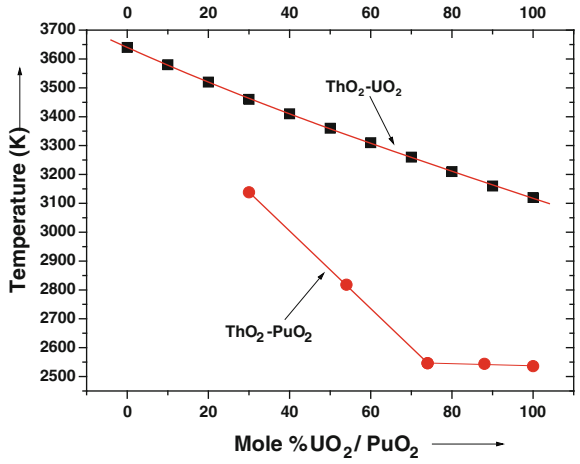

Fig. 3 Melting points of various compositions of ThO_2–UO_2 and ThO_2–PuO_2 system [12, 42]

3 Density

The fuel density, ρ is an important property of the fuel and is a function of the following factors: fuel composition, temperature, amount of porosity, O/M ratio, and burnup. The theoretical densities of the materials (ρ_T) can be calculated from the knowledge of lattice type and values of lattice parameter. Assuming that the elements form a solid solution, the theoretical density of the material can be calculated from the following relation [12]:

$$\rho_T = M_{\text{system}} N / (V N_a), \tag{1}$$

where, M_{system} is the atomic weight of the system, N the number of atoms per unit cell, V the volume of the lattice, and N_a the Avogadro constant. Thus, in the case of

a $(Th_{1-x}Pu_x)O_2$ solid solution, which is a fcc fluorite-type structure, with a lattice parameter a, the theoretical density can be estimated as :

$$\rho_T = 4[(1-x)M_{Th} + xM_{Pu} + 2M_O]/a^3N_a. \quad (2)$$

The density of a material as a function of temperature can be calculated using linear thermal expansion data obtained from a pushrod dilatometer, which measures thermal elongation of a material with respect to temperature (T). The relation between linear thermal expansion and density is expressed [40] as $\rho_0/\rho = (L/L_0)^3$, $L/L_0 \equiv (1 + \Delta L/L_0)$ (see Eq. (A.4) in Appendix 1 for details), so that one writes the fractional change in density as

$$\Delta\rho/\rho_0 \equiv [1-(L/L_0)^3]/(L/L_0)^3 = \left[1-(1+\Delta L/L_0)^3\right]/[1+\Delta L/L_0]^3, \quad (3)$$

where $\Delta\rho = \rho - \rho_0$ is the difference between densities at temperatures T and T_0.

In fluorite-type solid solutions, when the lattice parameter, a, and the molecular weight, M, are known, the theoretical density (Mg/m^3) can be calculated using the relation [12]:

$$\rho_T = 4M/\left(N_A a^3\right). \quad (4)$$

For pure ThO_2, the volume of the unit cell is $(0.55975\ nm)^3$ which is equal to $1.75381 \times 10^{-22}\ cm^3$. Density of pure ThO_2 at 298 K may, therefore, be calculated as $10.00\ g/cm^3$ [12]. The theoretical density of the ThO_2–UO_2 solid solution can be calculated from the following equation that makes use of Eq. (4) considering the additive rule for the molecular weights and cell volumes [39]:

$$\rho\left(Th_{1-y}U_yO_2\right) = 4[M_2 + y(M_1 - M_2)]/[N_A\left(a_2^3 + y\left(a_1^3 - a_2^3\right)\right], \quad (5)$$

where, M_1 and M_2 are the molecular weights of UO_2 and ThO_2, respectively, y is the molar fraction of UO_2 and a_1 and a_2 are the lattice parameters of UO_2 and ThO_2, respectively. The theoretical density of the ThO_2–UO_2 solid solution as a function of UO_2 content at 298 K is shown in Fig. 4.

The recommended equations for the density of solid uranium dioxide are based on the lattice parameter value of 0.54704 nm reported by Gronvold [46] at 293 K and thermal expansion data by Martin [47]. The above lattice parameter values are in good agreement with measurements by Hutchings [49] and are in full agreement with the recommendations of Harding et al. [48]. Assuming the molecular weight of UO_2 is 270.0277, this lattice parameter gives a density at 293 K as $10.956\ g/cm^3$. Applying the thermal expansion values of Martin [47], the density at 273 K is $10.963 \pm 0.070\ g/cm^3$. The values reported by Benedict et al. [51] and MATPRO for solid UO_2 are 10.970 ± 0.070 and $10.980 \pm 0.020\ g/cm^3$, respectively. Densities of UO_2 and PuO_2 given by various authors are shown in Table 4.

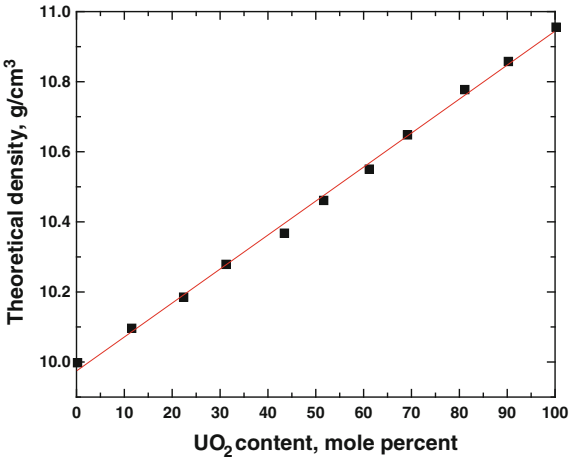

Fig. 4 Theoretical density of the ThO_2–UO_2 solid solution as a function of UO_2 content at 298 K [52]. (permission from Elsevier)

Table 4 Densities of UO_2 and PuO_2

	Density at 273 K (g/cm^3)	
	UO_2	PuO_2
Fink [50]	10.963 ± 0.070	
Benedict [51]	10.970 ± 0.070	11.460 ± 0.080
MATPRO [28]	10.980 ± 0.020	

From the data of coefficient of linear expansion, one can evaluate the fractional change in density of UO_2 or ThO_2 as a function of temperature up to their melting point. The following assumptions are considered:

1. There is no volume change on the formation of solid solution or solid solutions are ideal,
2. Densities of the solid solution can be calculated by evaluating the molar volume of the two components at the temperature of interest, and
3. Linear interpolation of the data to the desired temperature.

The density as a function of temperature may be calculated from [40]:

$$\rho_{(T)} = \rho_{(273)}\left[\left(L_{(273)}/L_{(T)}\right]^3, \tag{6}$$

where, $\rho_{(273)}$ is the density at 273 K; $L_{(273)}$ and $L_{(T)}$ are the lengths at 273 K and at temperature T (K), respectively. The ratio of length ($L_{(273)}/L_{(T)}$) can be calculated from the Martin's equation for the thermal expansion of UO_2 [47].

For 273 K $< T <$ 923 K,

$$L_{(T)} = L_{(273)}\left(9.9734 \cdot 10^{-1} + 9.802 \cdot 10^{-6} \cdot T - 2.705 \cdot 10^{-10} \cdot T^2 + 4.391 \cdot 10^{-13} \cdot T^3\right) \tag{7}$$

For 923 K $< T <$ 3,120 K,

$$L_{(T)} = L_{(273)}\left(9.9672 \cdot 10^{-1} + 1.179 \cdot 10^{-5} \cdot T - 2.429 \cdot 10^{-9} \times T^2 + 1.219 \cdot 10^{-12} \cdot T^3\right). \tag{8}$$

The density of solid stoichiometric UO_2 or mixed oxide (MOX) with a composition of UO_2–4 % PuO_2 as a function of temperature for the temperature range of 273–923 K is given by ORNL as [6]:

$$\rho_{(T)} = \rho_{(273)}\left(9.9734 \cdot 10^{-1} + 9.802 \cdot 10^{-6} \cdot T - 2.705 \cdot 10^{-10} \cdot T^2 + 4.391 \cdot 10^{-13} \cdot T^3\right)^{-3} \tag{9}$$

and the density of UO_2 or MOX for the temperature range of 923 K to the melting temperature,

$$\rho_{(T)} = \rho_{(273)}\left(9.9672 \times 10^{-1} + 1.179 \times 10^{-5} \cdot T - 2.429 \times 10^{-9} \cdot T^2 + 1.219 \times 10^{-12} \cdot T^3\right)^{-3} \tag{10}$$

The recommended uncertainty in the density value is 1 % in the entire temperature range.

Martin [47] recommends from assessment of the available data on hyperstoichiometric uranium dioxide (UO_{2+x}), using the same equations for the linear thermal expansion of UO_2 and of UO_{2+x} for x in the ranges 0–0.13 and 0.23–0.25. Therefore, Eqs. (9) and (10) are recommended for the density of UO_{2+x} for x in the ranges 0–0.13 and 0.23–0.25. No data on the effect of burnup on density or thermal expansion of UO_2 are currently available. In the absence of data, Eqs. (9) and (10) are recommended for UO_2 during irradiation, in accord with the recommendation of Harding et al. [48]. The density of UO_2 as a function of temperature is shown in Fig. 5.

As mentioned earlier, the phase diagram shows a continuous series of solid solutions between UO_2 and ThO_2. This is supported by the fact that deviations from Vegard's law are within the uncertainties of the lattice parameter measurements. Also, densities of ThO_2–UO_2 solid solution at room temperature can be calculated using additive rule:

$$\rho_{(273)} = 9.99003 + 0.00953 \cdot y \left(\text{in g/cm}^3\right), \tag{11}$$

where y is mol% UO_2.

The calculated theoretical densities, obtained from the measured lattice constants, for some ThO_2–UO_2 solid solution are given below in Table 5.

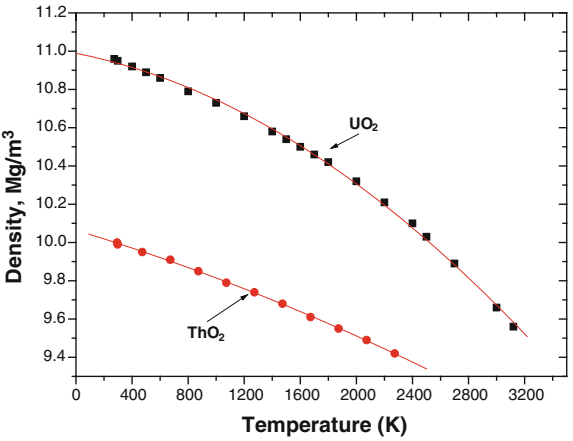

Fig. 5 Density of UO_2 [6, 31] and ThO_2 [40] as a function of temperature

Table 5 Room temperature lattice constants and theoretical densities of ThO_2–UO_2 solid solutions

Composition (mol% UO_2)	Lattice parameter (nm ± 0.00003 nm)	Theoretical density (g/cm^3)
0.0	0.55975	10.00
10.1	0.55846	10.09
20.2	0.55726	10.18
30.1	0.55590	10.28
40.3	0.55475	10.37
50.1	0.55355	10.46
60.1	0.55225	10.55
69.9	0.55098	10.65
80.1	0.54969	10.75
90.0	0.54841	10.85
100	0.54705	10.96

Belle and Berman [12] calculated theoretical density of ThO_2–UO_2 solid solution for different UO_2 content (x) from the lattice parameter data of Cohen and Berman [52]. The following equation shows the relationship between the theoretical density and UO_2 contents.

$$\rho_{(T)}\left(\mathrm{g/cm^3}\right) = 9.9981 + 0.0094 \cdot (x) - 8.7463 \cdot 10^{-6}(x)^2 + 1.1192 \cdot 10^{-7} \cdot (x)^3, \tag{12}$$

where, x is the UO_2 content.

Density of (Th, U)O_2 system has also been calculated as a function of temperature by many authors [12, 40, 53]. Momin and Venketeswarulu [54], Momin and Karkhanwala [55], Kempter and Elliott [56] and Springer et al. [57] reported the densities from the lattice and bulk expansion data. The density of (Th, U)O_2 system as a function of temperature and UO_2 content has been estimated from a

linear relationship of lattice parameters of (Th, U)O_2 as a function of UO_2 [12, 38, 57] at 298 K.

$$a_{298}(\text{nm}) = 0.55972 - 1.27819 \times 10^{-4}[\%\text{UO}_2] \tag{13}$$

A relationship for the average coefficient of linear thermal expansion in the temperature range 298–1,600 K as a function of UO_2 content was obtained from the literature using the high temperature lattice parameter measurements [12, 58–61]. Theoretical density was calculated as a function of UO_2 content using Eq. (12). Subsequently, the theoretical density was derived as a function of temperature and UO_2 content from the basic mass balance equation, i.e.,

$$\rho_T.V_T = \rho_0 \cdot V_0, \tag{14}$$

where, ρ_T, ρ_0, V_T, and V_0 are the densities and volumes at temperatures T and T_0, respectively.

With the coefficient of thermal expansion, the following equation was derived for the theoretical density [40]:

$$\begin{aligned}\rho_{(T)}\left(\text{g/cm}^3\right) = {} & 10.087 - 2.891.10^{-4} \times T - 6.354.10^{-7}(x) \times T \\ & + 9.279.10^{-3}(x) + 5.111.10^{-6} \times (x)^2,\end{aligned} \tag{15}$$

where x is UO_2 content. It is observed that the variation in density obtained from Eq. (15) and that from the literature is within ±0.28 %. The theoretical densities of UO_2 and ThO_2 at different temperatures are given in Table 6.

3.1 Density of Liquid UO_2

The recommended equation for the density of liquid uranium dioxide is based on the in-pile measurements of the vapor pressure, density, and isothermal compressibility of liquid (U, Pu)O_2 by Breitung and Reil [62]. Measurements of density as a function of enthalpy and as a function of temperature were obtained from the melting point to 7,600 K. The equation of Breitung and Reil for the

Table 6 Densities of ThO_2 and UO_2 as a function of temperature [12]

Temperature (K)	ThO_2 (g/cm^3)	UO_2 (g/cm^3)
298	10.00	10.96
473	9.95	10.90
673	9.89	10.83
873	9.83	10.76
1,073	9.78	10.69
1,273	9.72	10.62
1,473	9.66	10.55
1,673	9.60	10.48

density of UO_2 and (U, Pu)O_2 for mole fractions of Pu ≤ 0.25 is in good agreement with the equation for the density of UO_2 from experiments by Drotning [63], which had been recommended in the 1981 assessment by Fink et al. [64].

The recommended equation for the density of UO_2 as a function of temperature is:

$$\rho = 8.860 - 9.285 \cdot 10^{-4} \cdot (T - 3120), \tag{16}$$

where, density (ρ) is in g/cm^3 and temperature (T) is in K.

No data exists for the volume change of ThO_2 on melting, but some information is available on UO_2. Christensen [65] measured the density of UO_2 between 1,553 and 3,373 K by high-temperature radiography. The density of solid and liquid at 3,073 K were 9.67 and 8.74 g/cm^3, respectively. The accepted value of the density of liquid UO_2 at the melting point is 8.74 ± 0.016 g/cm^3. The volume increase on melting was 10.6 %.

Finally, the burnup also affects the density by the change in the porosity. At low burnup (<15 GWd/t), density increases by the fuel densification process; at the higher burnup, density decreases (porosity increases) due to the fuel swelling [66].

4 Thermal Expansion

As discussed earlier, the performance of a nuclear fuel is highly dependent on its physicochemical properties, especially their variation with temperature. One such property is thermal expansion of the fuel which affects the size of the gap between the fuel outer surface and cladding inner surface. The difference between the coefficients of thermal expansion of the fuel and the cladding determines whether the initial fuel–cladding gap closes or opens when the fuel element is brought to power [1]. If the initial gap is small and the fuel expands more than the cladding, the two come into contact. The resulting pressure at the interface is known as the contact or interfacial pressure. On the other hand, if the cladding expands more than the fuel and the gap is enlarged, heat conduction through the fuel–cladding gap will be low and the fuel temperature will be high because of the thermal resistance of the fuel–cladding gap. If interaction occurs, then differential thermal expansion between the fuel and cladding affects the magnitude of stresses in the cladding and fuel. This will be accounted for by including a thermal expansion strain component in the total strain of the fuel in each of three coordinate directions [1, 2, 4–6]. Fuel melting and excessive thermal expansion of the fuel pellet can occur at high enthalpy levels. The sudden expansion of the pellet can fail the cladding and resulting in molten fuel dispersion that can damage the pressure boundary. Dimensional changes are also affected by the processes such as sintering, bloating, or irradiation-induced changes such as swelling or densification [6]. For cubic crystals, such as ThO_2, UO_2, and ThO_2–UO_2 solid solutions, the

expansion or contraction is same in all directions. As long as phase changes do not occur, the dimensional changes are reversible [12].

The pellet–cladding mechanical interaction (PCMI) failures that occurred in the CABRI test reactor (France) and in the NSRR test reactor (Japan) were mainly due to rapid fuel thermal expansion because most of the energy remained in the fuel pellet during the extremely small time scale of the reactivity pulse [67]. With the same amount of energy deposition, thoria fuel will have a higher fuel temperature due to the lower heat capacity [12]. However, this high temperature does not necessarily lead to a larger thermal expansion because of the lower thermal expansion coefficient of thoria fuel. Results have shown that ThO_2–UO_2 fuel will have better performance than UO_2 fuel under Reactivity Initiated Accident (RIA) event conditions due to its lower thermal expansion and flatter power distribution in the fuel pellet [67].

Thermal dilation property of a material has correspondence to lowering in its density with temperature increase. The relative lowering in the density expressed in Eq. (3), leads to the following expression of the density ratio:

$$\rho/\rho_o = \{1 + [1 - (1 + (\Delta L/L_0)^3/(1 + (\Delta L/L_0)^3]\} \tag{17}$$

By Eq. (17), the density ratio can be evaluated from the linear dilation ($\Delta L/L_0$). Conversely, the relative dilation ($\Delta L/L_0$) can be determined using the following relation (see Appendix 1 for details) if density change is known,

$$(\Delta L/L_0) \approx (\rho_0/\rho)^{0.33} - 1 \tag{18}$$

The dilation property in a crystalline solid provides a measure of the extent of defect growth with temperature rise. The thermal expansion $\Delta L/L_0$ of a crystalline solid as per Eshelby theorem [12] can be written as:

$$\Delta L/L_0 = \Delta a/a_0 + 0.33\ \Delta N/N_0, \tag{19}$$

where a_0 is the lattice parameter at the reference temperature, $\Delta a = a_T - a_0$, N_0 is the number of occupied lattice sites at ambient temperature, and ΔN is the number of Schottky defects. The quantity becomes significant only at temperatures >0.6 Tm. By determining both $\Delta L/L_0$ and $\Delta a/a_0$ on the same specimen, it is possible to evaluate the energy of formation of Schottky defects. If, however, the thermally generated defects are of the Frenkel type, then thermal expansion will be same whether measured by XRD or by bulk measurements. The concentration of thermally generated Schottky defects in a cubic crystal can be determined from the above equation [12].

Further, the thermal dilation property is used in the evaluation of thermal stress in solid. In general, the total strain (ε) in a body is the sum of the mechanical strain (ε_M), and the thermal strain (ε_T) [1],

$$\varepsilon = \varepsilon_M + \varepsilon_T \tag{20}$$

$$\text{or, } \varepsilon = \sigma/E + \alpha \cdot \Delta T \tag{21}$$

where E is the Young's modulus and σ is the stress. In Eq. (21), it is assumed that both the elastic modulus, E, and the coefficient of thermal expansion, α, do not vary with temperature. The stresses due to change in temperature or due to temperature gradient are termed as thermal stresses, σ_{thermal} and can be expressed as:

$$\sigma_{\text{thermal}} = \alpha \cdot E \cdot \Delta T\,. \tag{22}$$

UO_2 and ThO_2 have the same isometric structure, and the ionic radii of 8-fold coordinated U^{4+} and Th^{4+} are similar (1.14 and 1.19 nm, respectively) [68]. Yamashita et al. [69] made the comparison for the linear thermal expansion coefficient (α) of actinide dioxides, using their measured values and literature ones at room temperature and at high temperature (1,200 K). They found that at room temperature the α values were almost the same of about $8.5 \times 10^{-6}\,K^{-1}$, but at high temperatures the α values increased with increasing atomic numbers from $10.2 \times 10^{-6}\,K^{-1}$ for ThO_2 to $13.2 \times 10^{-6}\,K^{-1}$ for BkO_2 [69, 70]. The thermal expansion coefficients of ThO_2, UO_2, and PuO_2 reported in the literature are shown in Table 7.

Lattice parameters of ThO_2, UO_2, and PuO_2 reported by various authors at room temperature are shown in Table 8.

It is well known that the lattice parameter (a) of nonstoichiometric UO_{2+x} diminishes with increasing excess oxygen content (x) and that the relation between a and x at room temperature is given as [12]

$$a(\text{pm}) = 547.05 - 9.4\,(x) \tag{23}$$

Values of linear thermal expansion (LTE) at temperature T can be calculated by the relation

$$\text{LTE}_{(T)}(\%) = (a_T - a_0) \times 100/a_0, \tag{24}$$

where, a_T is the lattice parameter at temperature T and a_0 is that at the reference temperature 293 K. The unit cell parameters could be determined as a function of temperature for ThO_2, UO_2, and PuO_2 with help of high temperature X-ray

Table 7 Thermal expansion coefficients of ThO_2, UO_2, and PuO_2 [69]

	ThO_2	UO_2	PuO_2
At 293 K ($\times 10^{-6}$)			
Yamashita et al. [69]	8.43	9.36	9.04
Marples [150]	7.3	9.3	8.4
Fahey et al. [151]	8.21	8.71	8.71
Taylor [71]	7.76	9.01	8.84
TPRC [61]	7.7	9.4	8.1
At 1,200 K ($\times 10^{-6}$)			
Yamashita et al. [69]	10.41	10.76	11.61
Fahey et al. [151]	10.24	12.35	12.14
Taylor [71]	11.00	11.31	12.27
TPRC [61]	10.4	11.6	12.00

Table 8 Lattice parameters of ThO_2, UO_2, and PuO_2 reported by various authors

	ThO_2 (pm)	UO_2 (pm)	PuO_2 (pm)	Year	Remarks
Zachariasen [152]	559.72 ± 0.05			1948	At 298 K
Gronvold [46]		547.04 ± 0.08		1955	At 293 K
Baldock et al. [153]		547.04 ± 0.01		1966	At 298 K
Marples [150]	559.68 ± 0.01	547.05 ± 0.01	539.60 ± 0.01	1976	At 292 K for PuO_2 At 293 K for ThO_2 At 294 K for UO_2
Taylor [71]	559.74	546.80	539.55	1984	At 298 K
Katz et al. [154]	559.7		539.60 ± 0.03	1986	At 298 K
Yamashita et al. [69]	559.74 ± 0.06	547.02 ± 0.04	539.54 ± 0.04	1997	At 298 K

diffractometer. Lattice parameters were measured with an accuracy of ±0.5 pm and are shown in Fig. 6.

Because of their technical importance as nuclear fuel, thermal expansions of ThO_2, UO_2 and PuO_2 have been intensively studied using various techniques (see Table 9). These data were compiled and assessed by Touloukian et al. [61]. They presented the recommended equations of the linear thermal expansion for ThO_2 and PuO_2 and the provisional equation for UO_2. Taylor [71], also, compiled and analyzed thermal expansion data and presented regression equations of lattice parameter as a function of temperature for these actinide dioxides.

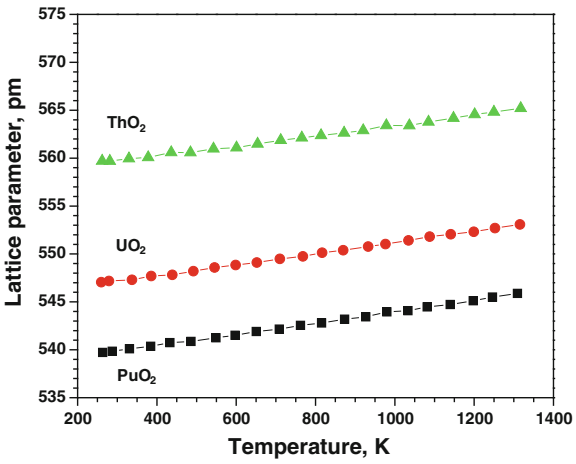

Fig. 6 Lattice parameters of ThO_2, UO_2, and PuO_2 as a function of temperature [69]. (permission from Elsevier)

Table 9 List of the authors worked on thermal expansion measurement on $(Th_{1-y}U_y)O_2$ system and year of publications

Year	Authors	Remarks
2012	Lu et al. [145]	Review based on first principles
2012	Bhagat et al. [85]	ThO_2 based SIMFUEL
2009	Subramaniam et al. [86]	ThO_2 containing 17.9, 41.7 and 52.01 % of $SmO_{1.5}$ in the temperature range 298–2,000 K
2008	Kutty et al. [84]	ThO_2–4 % UO_2, ThO_2–10 % UO_2 ThO_2–20 % UO_2
2006	Kim et al. [40]	Review paper
2006	Mathew et al. [87]	ThO_2–Nd_2O_3 phase with general compositions $Th_{1-x}Nd_xO_{2-x/2}$
2005	Grover et al. [88]	(Th, Ce, Zr)O_2
2001	Mathew et al. [89]	ThO_2, $Th_{0.96}Ce_{0.04}O_2$, $Th_{0.92}Ce_{0.08}O_2$
2000	Fink [64]	Review paper
2000	Anthonysamy et al. [78]	$(Th_{0.45}U_{0.55})O_2$, $(Th_{0.87}U_{0.13})O_2$ and $(Th_{0.09}U_{0.91})O_2$
2000	Tyagi and Mathew [77]	ThO_2 and ThO_2–2 wt% UO_2
1997	Bakker et al. [38]	Review paper
1991	Momin et al. [60]	High temperature XRD on ThO_2 and $(Th_{0.8}U_{0.2})O_2$
1991	Momin et al. [60]	ThO_2 and $(Th_{0.8}U_{0.2})O_2$ with 20 wt% Ln_2O_3.
1988	Martin [47]	Review paper
1981	Rodrigues and Sundaram [82]	Review paper
1977	Hirata et al. [75]	ThO_2 having 99.99 % purity
1970	Touloukian et al. [61]	Review paper
1967	Springer et al. [79]	ThO_2–10.09 % UO_2 and ThO_2–20.02 mol% UO_2 in temperature range 293–2,273 K
1967	Turner and Smith [80]	(U, Th)O_2 where U: Th = 1:10, 293–1,273 K
1962	Lynch and Beals [81]	<1,173 K
1959	Kempter and Elliot [56]	ThO_2–50.05 % UO_2 in temperature range 293–1,173 K
1959	Powers and Sharpio [83]	$(Th_{0.936}U_{0.064})O_2$, <1,073 K

4.1 ThO_2

The thermal linear expansion of ThO_2 is well established. Touloukian et al. [61] list more than 34 different experimental determinations which are in excellent agreement and recommended the following equation (150–2,000 K):

$$\%\,\Delta L/Lo = -0.179 + 5.097 \times 10^{-4}(T/K) + 3.732 \times 10^{-7}(T/K)^2 - 7.594 \times 10^{-11}(T/K)^3, \quad (25)$$

Touloukian states that the equation has an accuracy of ±3 % or less. Hoch and Momin [72] showed that their data, obtained by XRD measurements of thermal expansion of ThO_2, is in very good agreement with that obtained by Ohnysty and

Table 10 Recommended values for linear thermal expansion of ThO_2 [12]

Temperature (K)	$\%\Delta L/L_0$	Expansion coefficient, $\times 10^{-6}$ K^{-1}	
		Mean	Instantaneous
298.15	0.0	8.43	8.43
400	0.087	8.53	8.63
500	0.174	8.63	8.82
600	0.264	8.73	9.01
700	0.355	8.83	9.20
800	0.448	8.93	9.39
1,000	0.641	9.13	9.77
1,200	0.842	9.33	10.2
1,400	1.05	9.53	10.5
1,600	1.27	9.73	10.9
1,800	1.49	9.93	11.3
2,000	1.72	10.1	11.6
2,500	2.34	10.6	12.5
3,000	3.01	11.1	13.4
3,500	3.72	11.6	14.3

Rose [73] by dilatometry. Their data also agreed well with that of Aronson et al. [74] and Hirata et al. [75]. Hoch and Momin [72] recommended the following equation for ThO_2 (293–2,373 K):

$$\% \Delta L/L_0 = -0.2426 + 7.837 \times 10^{-4}(T/K) + 9.995 \times 10^{-8}(T/K)^2 \qquad (26)$$

The results obtained from the above equations are almost identical. Hoch and Momin concluded from their studies that the lattice defects in ThO_2 were probably of the Frenkel type.

The extrapolation data to higher temperatures other than those covered by measurements need caution [76]. The equation of Touloukian is valid in the range of 150–2,000 K and that of Hoch and Momin [72] should be used for extrapolation. The recommended values of thermal expansion of are shown in Table 10. Thermal expansion curve for ThO_2 is shown in Fig. 7.

4.2 UO_2

Martin [47] had reviewed 15 sets of UO_2 thermal expansion data and provided a relation which has been accepted as the most authenticated data. Fink in her peer review paper [64] on thermophysical properties of UO_2 has also recommended the data suggested by Martin. Recommended percentage linear thermal expansion for UO_2 by Martin [47]:

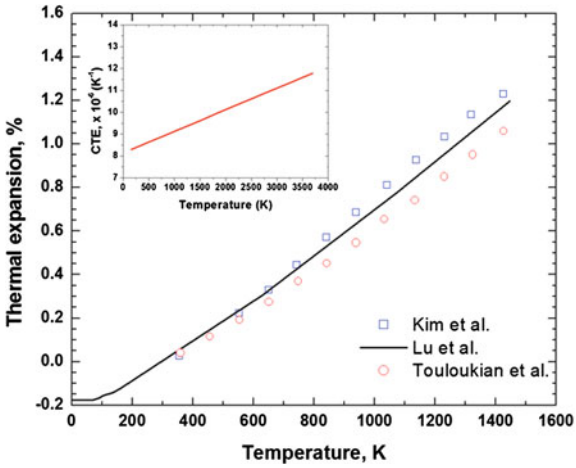

Fig. 7 Temperature dependence of the linear thermal expansion for ThO_2 [145]. The inset is the volume thermal expansion coefficient as a function of temperature [12]

$$(\Delta L/L_0) \times 100 = -0.266 + 9.802 \times 10^{-4} \cdot T - 2.705 \times 10^{-8} \cdot T^2 + 4.391 \times 10^{-11} \cdot T^3, \quad (27)$$

$(273\ \text{K} < T < 923\ \text{K})$.

$$(\Delta L/L_0) \times 100 = -0.328 + 1.179 \times 10^{-3} \cdot T - 2.429 \times 10^{-7} \cdot T^2 + 1.219 \times 10^{-10} \cdot T^3, \quad (28)$$

$(923\ \text{K} < T < 2{,}000\ \text{K})$.

Figure 8 shows a plot of expansion in percentage versus temperature for both ThO_2 and UO_2 and it shows that ThO_2 has a lower expansion than UO_2.

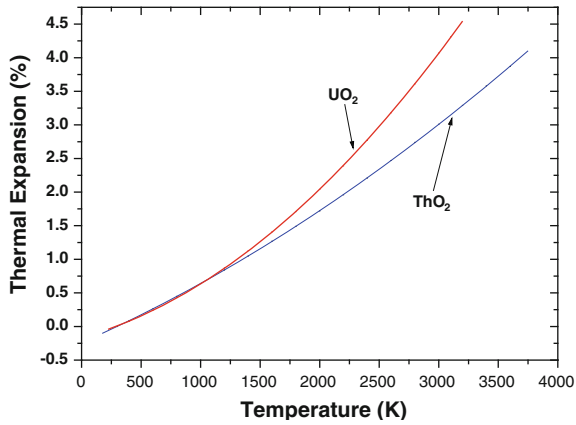

Fig. 8 Comparison of thermal expansion of ThO_2 and UO_2. Data of Belle et al. are re-plotted and shown above [12]

4.3 ThO_2–UO_2

Substitution of uranium for thorium in ThO_2–UO_2 system results in the decrease of lattice parameter, melting point, oxygen potential, thermal conductivity, while the density and the linear thermal expansion show an increase. In the uranium concentration range $y > 0.2$, less data are available but the same trend is expected. It was mentioned earlier that, at room temperature, the lattice parameter decreases linearly from 100 % ThO_2 to 100 % UO_2. Based on the results of calorimetric studies, thermal expansion studies, and other thermodynamic measurements on urania–thoria solid solutions [40], it is suggested that stoichiometric urania–thoria solid solutions are nearly ideal at least up to 2,000 K. Therefore, one can assume that this linear decrease in the lattice parameter also exists at high temperature. This linear decrease can only exist when the linear thermal expansion of $(Th_{1-y}U_y)O_2$ $(0 < y < 1)$ equals the linearly interpolated value of that of ThO_2 and that of UO_2.

The thermal linear expansion of the $(Th_{1-y}U_y)O_2$ solid solution has been studied in much less detail than that of the pure compounds. Konings et al. [39] reviewed the thermophysical properties of ThO_2-based fuels. They concluded from the results of eight studies on $(Th_{1-y}U_y)O_2$, and suggested the equation of the type:

$$\begin{aligned}\Delta L/L_0 = {} & \left(8.1635 \times 10^{-4} + 3.8325 \times 10^{-4} y + 5.2423 \times 10^{-4} y^2\right)(T/K - 298.15) \\ & + \left(1.2144 \times 10^{-7} + 1.4936 \times 10^{-8} y + 1.5633 \times 10^{-7} y^2\right)(T/K - 298.15)^2,\end{aligned} \tag{29}$$

where, the thermal linear expansion $\Delta L/L_0$ in %, and y is the molar fraction of UO_2.

Bakker et al. [38] have recommended the percentage linear thermal expansion data of $(Th_{1-y}U_y)O_2$ $(0 < y < 1)$ by obtaining the linear interpolation of the values of Touloukian [61] and Martin [47] and obtained the following relations in two different set of temperature ranges:

$$\begin{aligned}(\delta L/L_0) \times 100 = {} & -0.179 - y\,0.087 + \left(5.097 \times 10^{-4} + y\,4.705 \times 10^{-4}\right) \cdot T \\ & + \left(3.732 \times 10^{-7} - y\,4.002 \times 10^{-7}\right) \cdot T^2 \\ & - \left(7.594 \times 10^{-11} - y\,11.98 \times 10^{-11}\right) \cdot T^3\end{aligned} \tag{30}$$

$$(\text{for } 273\ \text{K} < T < 923\ \text{K}),$$

$$\begin{aligned}(\Delta L/L_0) \times 100 = {} & -0.179 - -y\,0.149 + \left(5.097 \times 10^{-4} + y\,6.693 \times 10^{-4}\right) \cdot T \\ & + \left(3.732 \times 10^{-7} - y\,6.161 \times 10^{-7}\right) \cdot T^2 \\ & - \left(7.594 \times 10^{-11} - y\,19.784 \times 10^{-11}\right) \cdot T^3\end{aligned} \tag{31}$$

$$(\text{for } 923\ \text{K} < T < 2{,}000\ \text{K}).$$

Momin et al. [60] measured lattice thermal expansion of (Th, U)O_2 system by X-ray diffraction method. They obtained coefficient of expansion data for pure ThO_2 and $(Th_{0.8}U_{0.2})O_2$ to be 9.5 × 10^{-6} K^{-1} and 7.1 × 10^{-6} K^{-1}, respectively, in the temperature range 298–1,600 K. It was observed that the coefficient of thermal expansion of $(Th_{0.8}U_{0.2})O_2$ is lower than either of ThO_2 and UO_2, which is quite unreasonable.

Tyagi et al. [77] found CTE values for ThO_2 and ThO_2–2 wt% UO_2 to be 9.58 × 10^{-6} and 9.74 × 10^{-6} K^{-1}, respectively, in the temperature range of 298–1,473 K. The CTE value reported in IAEA-TECDOC [40] for ThO_2 in the temperature range 300–1,473 K is 9.732 × 10^{-6} K^{-1} and for ThO_2–4 wt% UO_2 it is 9.85 × 10^{-6} K^{-1}; both these values were found to be in close agreement with those reported by Tyagi et al. The CTE value 10.33 × 10^{-6} K^{-1} for composition $(Th_{0.87}U_{0.13})O_2$ in the temperature range 298–1,973 K as reported by Anthonysamy et al. [78] matches well with the value obtained in the IAEA study for ThO_2–10 % UO_2 which was found to be 10.21 × 10^{-6} K^{-1} in the temperature range 300–1,773 K. The average linear thermal expansion coefficients for $(Th_{0.45}U_{0.55})O_2$ and $(Th_{0.09}U_{0.91})O_2$ were measured to be 10.83 × 10^{-6} K^{-1} and 11.45 × 10^{-6} K^{-1}, respectively, in the temperature range between 298 and 1,973 K. These data clearly show that thermal expansion coefficients increases with increase in UO_2 content in ThO_2–UO_2 system. Figure 9 shows % thermal expansion plot of some typical ThO_2–UO_2 solid solutions.

The coefficient of expansion data of Momin et al. [60], Springer et al. [79], Turner and Smith [80], Kempter and Elliot [56] and Lynch and Beals [81] show a wide scatter of data points when plotted against composition. Rodriguez and Sundaram [82] in their review article reported an average linear thermal expansion coefficient of 9.67 × 10^{-6} K^{-1} for ThO_2 (293–2,273 K) and 12.5 × 10^{-6} K^{-1} for $(Th_{0.8}U_{0.2})O_2$ (1,100–2,400 K). Powers and Shapiro [83] reported the same average linear thermal expansion coefficient value of 9 × 10^{-6} K^{-1} for both pure

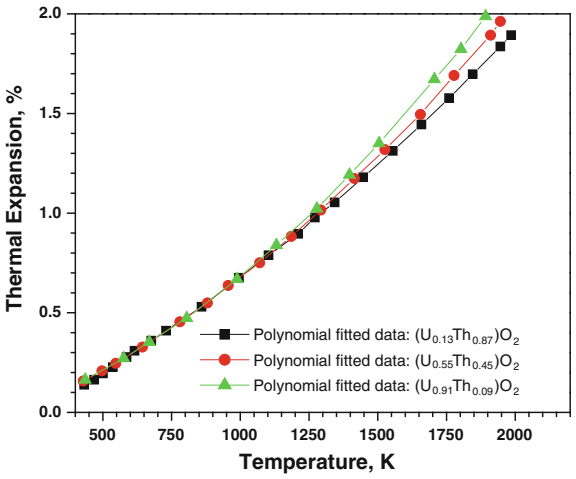

Fig. 9 Percent thermal expansion plot of some typical ThO_2–UO_2 solid solutions [78]. (permission from Elsevier)

UO_2 and $(U_{0.064}Th_{0.936})O_2$. They obtained lower coefficient value (8×10^{-6} K^{-1} up to 1,073 K) for $(Th_{0.8}U_{0.2})O_2$.

Kutty et al. [84] measured thermal expansion of ThO_2, ThO_2–4 % UO_2, and ThO_2–20 % UO_2 pellets fabricated by (Coated Agglomerate Pelletization) CAP route using ThO_2 and U_3O_8 powders as the starting materials. They reported that the thermal expansion of ThO_2–20 % UO_2 pellet was different from that of ThO_2 and ThO_2–4 % UO_2, e.g., it increased more rapidly with increasing temperature in the temperature range of 1,000–1,500 °C which they attributed to the loss of oxygen of (Th, U)O_{2+x} above 1,000 °C. The thermal expansion behavior of polycrystalline samples of ThO_2–3.45 % UO_2 and SIMFUEL corresponding to the burnup of 43,000 MWd/Te has been investigated from room temperature to 1,473 K, and for SIMFUEL corresponding to burnup of 28,000 MWd/Te has been investigated from room temperature to 1,173 K, using a high-temperature X-ray diffraction (HTXRD) by Bhagat et al. [85]. They reported that SIMFUEL has higher thermal expansion than ThO_2–3.45 % UO_2 and this is related to the higher thermal expansion coefficient of dissolved rare earth oxides and also to the lower melting point of SIMFUEL matrix.

The mean linear thermal expansivity for ThO_2–$SmO_{1.5}$ solid solutions containing 17.9, 41.7 and 52.01 % of $SmO_{1.5}$ were determined by Subramanian et al. [86] in the temperature range 298–2,000 K. The mean linear thermal expansion coefficients for ThO_2–$SmO_{1.5}$ solid solution were found to be 10.47, 11.16, and 11.45×10^{-6} K^{-1}, respectively. The synthesis, characterization, and lattice thermal expansion studies of the ThO_2–Nd_2O_3 phase with general compositions $Th_{1-x}Nd_xO_{2-x/2}$ are reported by Mathews et al. [87]. The lattice thermal expansion (293–1,473 K) behavior of the solid solutions has been investigated by high temperature XRD and found to show a gradual increase with increasing content of $NdO_{1.5}$ in $Th_{1-x}Nd_xO_{2-x/2}$ series. The lattice thermal expansion behavior of a number of single-phase compositions of CeO_2–ThO_2–ZrO_2 in the temperature range from 293 to 1,473 K, as investigated by high-temperature XRD are reported by Grover et al. [88]. The average lattice thermal expansion coefficient of pure thoria was found to be 9.58×10^{-6} K^{-1}, which increased to 11.91×10^{-6} K^{-1} in the composition$Th_{0.05}Ce_{0.90}Zr_{0.05}O_2$.

Momin et al. [60] studied thermal expansion behavior of ThO_2 and $(Th_{0.8}U_{0.2})O_2$ with 20 wt% Ln_2O_3. Ln_2O_3 contained oxides of La, Nd, Ce, Y, Sm, Gd, and Eu in equal proportions. Authors found that average thermal expansion coefficient of the solid solutions of ThO_2 and $(Th_{0.8}U_{0.2})O_2$ with 20 wt% Ln_2O_3 show an increase as compared to those of the parent compounds. Authors related the higher values of coefficient of expansion to the partial substitution of U^{4+} or Th^{4+} with Ln^{3+} resulting in weakening the interatomic bonding in the solid solution matrix. Grover et al. [88] found that coefficient of linear thermal expansion of (Th, Ce, Zr)O_2 is higher than ThO_2 and increases with increase of cerium and zirconium content in (Th, Ce, Zr)O_2. Dilatometric measurement on ThO_2–10.09 % UO_2 and ThO_2–20.02 mol% UO_2 by Springer et al. [79] and XRD determination on ThO_2–50.05 % UO_2 by Kempter and Elliot [56] have been reported. Variation in expansion with composition in any case is reported to be quite small.

4.4 ThO_2–PuO_2

ThO_2 and PuO_2 form a continuous series of solid solutions over the entire range of composition. At the Pu-rich end, mixed oxide may be heterogeneous if prepared under reducing conditions, as a result of the formation of Pu_2O_3. The lattice parameter of $(Th_{1-y}Pu_y)O_2$ decreases linearly from pure ThO_2 to pure PuO_2 [26]. Lattice parameters of (Th, Pu)O_2 with various PuO_2 contents are given in Table 11. Assuming ideal solid solution behavior at high temperatures for ThO_2 and PuO_2, it would be expected that this linear decrease in lattice parameter would also happen at elevated temperatures.

The available data on ThO_2–PuO_2 are scanty. One way to overcome this problem is to use CeO_2 in place of PuO_2 as they both have quite similar physico-chemical properties viz., ionic radii in octahedral and cubic coordination, melting points, standard enthalpy of formation and specific heat etc. Thus, the plutonium chemistry can be well simulated using CeO_2 in place of highly active PuO_2. Mathews et al. [89] have recently measured bulk thermal expansion of (Th, Ce)O_2 system. Bulk and lattice thermal expansion studies on $(Th_{1-y}Ce_y)O_2$ ($y = 0.0$, 0.04, 0.08 and 1.0) were carried out by dilatometry and high temperature XRD from room temperature to 1,123 and to 1,473 K, respectively. The average linear thermal expansion coefficients of ThO_2, $Th_{0.96}Ce_{0.04}O_2$, $Th_{0.92}Ce_{0.08}O_2$, and CeO_2 were found to be 9.04×10^{-6}, 9.35×10^{-6}, 9.49×10^{-6}, and 11.58×10^{-6} K^{-1}, respectively, between 293 and 1,123 K. Some data on $(Th_{1-y}Pu_y)O_2$ generated at BARC was reviewed in IAEA-TECDOC [40]. Thermal expansion curve for $(Th_{1-y}Pu_y)O_2$ for $y = 0.02$, 0.04, 0.06, 0.10 are shown in Fig. 10.

The thermal expansion of the solid solutions $(Th_{1-y}Pu_y)O_2$ could be reasonably approximated at various temperatures by taking linear interpolated expansion data of ThO_2 and PuO_2 as per their weight fraction. IAEA-TECDOC [40] used "interpolation method," using the recommended equation by Touloukian [61] for ThO_2 and the following equation for pure PuO_2 as recommended by MATPRO. The equation for linear strain calculations is as given below:

$$\varepsilon = K_1 \cdot T - K_2 + K_3 \cdot \exp(-E_D/k_B T), \tag{32}$$

Table 11 Lattice parameter of ThO_2–PuO_2 solid solution at 298 K [26]

PuO_2 (mol%)	Lattice parameter (pm)
0	559.6 ± 0.1
15	556.8 ± 0.4
26	554.62 ± 0.04
36.9	552.6 ± 0.1
46.7	550.2 ± 0.1
63.5	546.93 ± 0.04
82.5	542.8 ± 0.1
100	539.60 ± 0.03

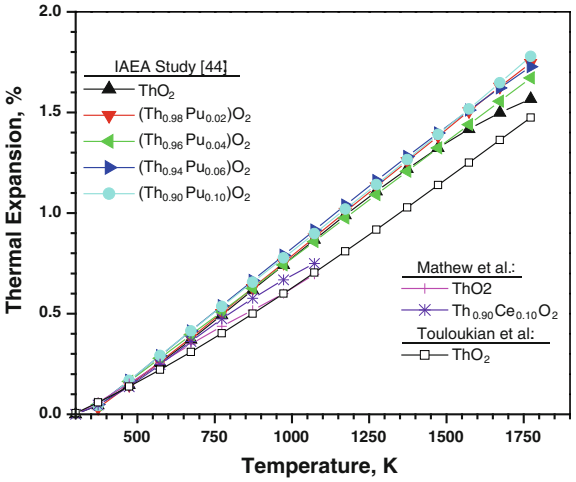

Fig. 10 Thermal expansion curves for $(Th_{1-y}Pu_y)O_2$ for $y = 0.02$, 0.04, 0.06 and 0.10 [40]. (permission from IAEA)

where, ε is the linear strain which is taken as zero at 300 K, T is the temperature (K), k_B is Boltzman's constant (1.38×10^{-23} J/K), and E_D, K_1, K_2, and K_3 are constants having values 7×10^{-20} (J), 9×10^{-6} (K^{-1}), 2.7×10^{-3} (unit less), and 7×10^{-2} (unit less), respectively.

Percentage linear thermal expansion for $(Th_{1-y}Pu_y)O_2$ ($0 < y < 1$) obtained by linear interpolation of the data of ThO_2 and data for PuO_2 and can be expressed as (in the temperature range of 300–1,773 K) [40].

$(Th_{1-y}Pu_y)O_2$ where $0 < y < 1$:

$$\begin{aligned}(\Delta L/L_0) \times 100 = &-0.179 - 0.049 \cdot y + \left(5.079 \times 10^{-4} + 2.251 \times 10^{-4} \cdot y\right) \cdot T \\ &+ \left(3.732 \times 10^{-7} - 2.506 \times 10^{-7} \cdot y\right) \cdot T^2 \\ &+ \left(-7.594 \times 10^{-11} + 12.454 \times 10^{-11} \cdot y\right) \cdot T^3\end{aligned} \tag{33}$$

As part of thorium-based fuel development program for fast breeder reactors, the thermophysical properties of mixed thorium–plutonium oxide pellets of both thorium- and plutonium-rich compositions were evaluated in India [58]. The plutonium-rich mixed oxide pellets contained 70–80 % PuO_2 which could be considered as candidate fuel for small LMFBR core like the operating fast breeder test reactor (FBTR). The thorium-rich compositions contained 20–30 % PuO_2 which could be considered as alternative fuel for large LMFBRs like the forth-coming prototype fast breeder reactor (PFBR-500). The mixed oxide pellets were prepared by "powder-pellet" route involving mechanical mixing of ThO_2 and PuO_2 powders followed by cold pelletization and high temperature sintering. Small amount of Nb_2O_5 (0.25 wt%) or CaO (0.5 wt%) powder were used as "sintering aid" and admixed with the powder during co-milling. The coefficient of thermal expansion of mixed $(Th_{0.3}Pu_{0.7})O_2$, $(Th_{0.7}Pu_{0.3})O_2$, and $(Th_{0.8}Pu_{0.2})O_2$

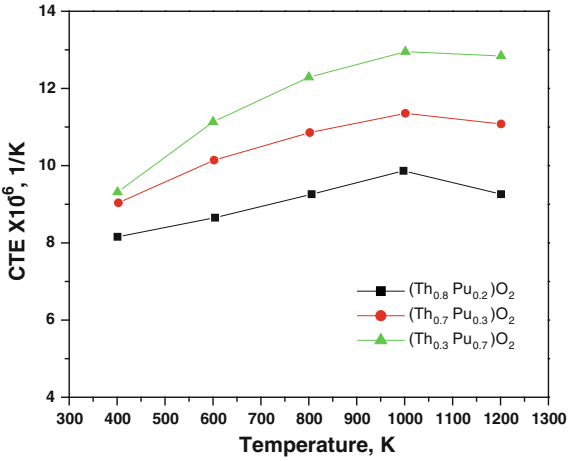

Fig. 11 Thermal expansion curves for high Pu bearing $(Th_{1-y}Pu_y)O_2$ samples [58]. (permission from IAEA)

were evaluated by a high-temperature dilatometer and is summarized in Fig. 11. XRD pattern of ThO_2 and the pellets containing lower amounts of PuO_2 (30 % PuO_2) sintered in either Ar or Ar-8 % H_2 showed only single-phase isostructural with fluorite phase. But ThO_2–PuO_2 pellets with higher plutonium content such as ThO_2–50 % PuO_2 and ThO_2–75 % PuO_2 pellets sintered in either Ar or Ar-8 % H_2 showed the presence of two phases. In addition to the phase that is isostructural with PuO_2 (fluorite), another phase which is isostructural with bcc α-Pu_2O_3 has been observed [90]. Hence, no conclusion could be drawn from the above results.

5 Thermal Conductivity

Among the various thermal properties, thermal conductivity is the most useful property for the nuclear scientist. It is the ability of the material to transfer heat from a region of high temperature to a region of low temperature. In normal conditions, thermal conductivity and linear power determine the peak fuel operating temperature. Under the accident conditions, the thermal conductivity of the fuel determines the maximum permissible linear rating, χ_{max}, if central melting is to be avoided [10, 38]. The thermal conductivity, λ, allows the determination of centre temperature of fuel, T_c, when the surface temperature T_s, is known by using the conductivity integral,

$$\chi = 4\pi \int_{T_s}^{T_c} \lambda dT \tag{34}$$

where χ is the linear rating.

For ceramic oxide systems, two contributions are used to describe the behavior of thermal conductivity with temperature: (i) the phonon–phonon interaction and (ii) the density of defects (phonon scattering centers) in the lattice [91]. For temperatures below 1,900 K, the contribution of the free electrons to the thermal conductivity can be neglected.

5.1 Fundamental Relations in Thermal Conductivity

According to kinetic gas theory, the lattice thermal conductivity above Debye temperature for an ideal lattice can be expressed by [12]

$$\lambda_l = 0.33\, C_v v L \tag{35}$$

where, C_v is the specific heat at constant volume, J/m^3·K, v is the velocity of sound in solid, m/s, and L is the mean free path of scattered waves (the phonon wavelength), m.

Above the Debye temperature, thermal conductivity of electric insulators decreases with increasing temperatures. Since atomic vibrational frequency increases with temperature, an increase in wave scattering is anticipated which are shown to be due to phonon interaction. Thermal energy is transferred by the Umklapp process, in which two phonons interact to form a third [12]. According to this theory, lattice thermal conductivity is inversely proportional to absolute temperature and this becomes a minimum when phonon wavelength becomes less than the mean distance between the scattering centers. For crystalline solid, the minimum distance between the scattering centers is the interatomic distance which is the lattice parameter, a_o. Therefore, the above equation becomes [12]:

$$(\lambda_l)_{\min} = 0.33\, C_v v a_o \tag{36}$$

In solids, phonon–phonon scattering is due to the anharmonic components of crystal vibrations. Lattice anharmonicity increases with the mass difference between anions and cations in the ionic material and is greatest in UO_2 or PuO_2 [38, 91]. As a result, the thermal conductivity of the oxides of the actinide metals is considerably lower than that of most other crystalline oxides. The kinetic theory of gases shows that the collision mean free path is given by the reciprocal of the product of the collision cross-section σ_P and the density of scattering points (n_P):

$$L = (1/\sigma_P n_P) \tag{37}$$

The deviation from stoichiometry and the presence of foreign atoms or porosity result in lower values of λ in actinide oxides. Further, it can be shown that the phonon mean free path should vary as $1/T$. In general, phonon–phonon scattering and phonon–impurity scattering are the dominant mechanisms of the thermal

conductivity in ceramics. Klemens [92] has proposed a heat conduction model in materials where the phonon–phonon (Umklapp) scattering and the phonon–impurity scattering occur simultaneously. Theoretically, the phonon component of the thermal conductivity λ may be written as:

$$\lambda = (A + \mathrm{BT})^{-1} \tag{38}$$

where A and B are constants and T is the absolute temperature.

Thermal resistivity (R), which is the reciprocal of thermal conductivity (λ), of the above oxides can be described by the following equation:

$$R = 1/\lambda = A + \mathrm{BT} \tag{39}$$

The first term, A, in Eq. (39) represents the defect thermal resistivity. This results from the phonon interactions with lattice imperfections, impurities, isotopic, or other mass differences as well as bulk defects such as grain boundaries in the sample. The influence of substituted impurities on the thermal conductivity is described by the increase of the parameter A. The second term in Eq. (39), namely BT, represents the intrinsic lattice thermal resistivity caused by phonon–phonon scattering [1, 2]. As the temperature increases, this term becomes predominant. The parameter B remains nearly constant by substitution. The constants A and B can be obtained from the least squares fitting of the experimental data.

The thermal conductivity of nuclear ceramics is strongly influenced by the stoichiometry. Deviations from stoichiometry produce point defects, most likely oxygen vacancies or metal interstitials in hypostoichiometric compounds and oxygen interstitials or metal vacancies in hyperstoichiometric compounds. Introduction of point defects into the oxygen ion sublattice or substitution of Th for U on the cation sublattice provides additional centers from which phonon scattering occurs. It is reported that there is a drastic change in the uranium vacancy concentration on varying O/M ratio around the stoichiometric composition. Many reports are available on the effect of stoichiometry on the thermal conductivity of UO_2 and (U, Pu)O_2 samples [1]. Thermal conductivities decrease as their hyperstoichiometry, x, increases. At low temperatures, thermal conductivity of mixed oxide can be described by a modified equation of (38) as [93, 94]:

$$\lambda = 1/[A(x,q) + B(x,q)T] \tag{40}$$

where, x and q denote the extent of nonstoichiometry and the Pu/Th content in the UO_2 lattice, respectively. The limited amount of experimental information available suggests that the coefficient A depends primarily on the O/M ratio and only very weakly on the plutonium content. The coefficient A may be written as

$$A = A_0 + \Delta A(x) \tag{41}$$

where, A_0 is very nearly equal to the A value of pure UO_2. The perturbation ΔA arises from interactions of point defects with lattice. The magnitude of ΔA is proportional to the defect atom fraction and to a measure of the cross section of the

defect for phonon scattering. The latter is proportional to the square of the difference between the atomic radius of the defect (r_1) and that of the host atom (r). The mass difference between the impurity atom and the host atom may also influence A, but this contribution is not significant in mixed oxide fuel materials. A can also be represented by the following equation as

$$A = \left[(\pi^2 V\theta)/\left(3\mathrm{hv}^2\right)\right] \sum_i \Gamma_i, \tag{42}$$

where V, θ, h, and v denote the average atomic volume, Debye temperature, Planck's constant, and phonon velocity, respectively. The term $\Sigma_i\Gamma_i$ is the sum of the cross-sections of all the phonon-defect scattering centers. The analysis of the lattice defect thermal resistivity and the evaluation of phonon scattering by the various defect scattering centers in pure and mixed actinide oxides have been carried out by several authors [91–94]. Accordingly, A of Eq. (42) can be given as

$$A = C(\Gamma_u + \Gamma_o), \tag{43}$$

where $C = (\pi^2 V\theta)/(3\mathrm{hv}^2)$. Γ_u is the scattering cross-section arising from U substitution and Γ_o is that from all other native defects present in the sample. The scattering cross-section Γ_u can be expressed in terms of the mass and size difference of the substituted atom over that of the host [95]:

$$\Gamma_u = x(1-x) \times \left[(\Delta M/M)^2 + E(\Delta r/r)^2\right], \tag{44}$$

where, x is atomic fraction of substituted U in place of Th, ΔM and Δr are the mass and radius difference between U and Pu/Th atom, respectively, M and r are average mass and radius of the substituted atom, and E is an adjustable parameter which represents the magnitude of lattice strain. From the above, it is clear that scattering cross-section depends upon the mass difference between Th and U atoms, size difference between Th and U atoms, charge of U ion and microstructure.

Thermal transport by electrical charge carriers can also contribute to thermal conduction at high temperatures. The ratio between thermal and electrical conductivities of metals can be expressed in terms of the ratio:

$$L_c = \lambda/\sigma T = \pi^2 k^2/3e^2 = 2.45 \times 10^{-8}\, W\Omega/K^2, \tag{45}$$

which may be called the Wiedemann–Franz ratio or the Lorenz constant. In the above equation, σ is the electrical conductivity, e is the electronic charge, and k is Boltzmann's constant. Thermal conductivity of a solid can be measured by two methods:

1. By determining the stationary heat flow through the specimen, which gives λ directly,
2. By determining the variation of the temperature at a fixed plane, that is a specimen surface, due to an induced nonstationary heat flow which gives the thermal diffusivity, α.

Since the second method is more versatile and requires smaller specimen, it has become a standard method for determining λ for $T > 600$ K. For lower temperatures, the first method is more suited.

For the thermal diffusivity measurement, the sintered pellet was sliced into discs of about 10 mm diameter and 2 mm thickness using a low speed cut-off wheel. A pulse of laser was projected on to the front surface of the pellet and the temperature rise on the rear side of the pellet was recorded as a transient signal by using an infrared detector. The thermal diffusivity (α_t) was calculated from the following relationship:

$$\alpha_t = WL^2/\pi t_{1/2} \tag{46}$$

where $t_{1/2}$ is the time required in seconds to reach half of the maximum temperature rise at the rear surface of the sample and L is the sample thickness in millimeter. W is a dimensionless parameter which is a function of the relative heat loss from the sample during the measurement. The data have to be corrected for radiation heat losses by the method of Clark and Taylor [96].

Unlike UO_2 or PuO_2, ThO_2 is a semitransparent material to wavelengths of the infrared region. For a laser flash experiment, all the energy of the laser pulse is not absorbed on the front face of the sample, but also in volume. Also, the temperature measurement on the rear face is skewed as the pyrometer may receive radiation produced not only at the sample surface, but also in volume. These difficulties are overcome if the faces of the samples are given a coating by graphite. A coating of graphite on both faces was used in order to make sure that the energy of the laser is absorbed on the front face and to improve the temperature recording on the rear face.

Heat transport through materials is described by two properties: thermal conductivity, λ (under steady state conditions) and thermal diffusivity, α_t (under transient conditions). These two properties are related by the expression:

$$\lambda(T) = \alpha_t(T) \cdot \rho(T) \cdot C_p(T)\,, \tag{47}$$

Where, ρ the density of the material and C_p its specific heat at constant pressure. The specific heat of mixed oxide like $(Th_{1-y}Pu_y)O_2$ solid solutions was calculated from the literature values of specific heats of pure ThO_2 and PuO_2 and subsequently using Neumann–Kopp's rule. The following equations were used to calculate C_p of $(Th_{1-y}Pu_y)O_2$:

$$C_p\left(\mathrm{Th}_{1-y}\mathrm{Pu}_y\right)O_2 = (1-y) \cdot C_p(\mathrm{Th}O_2) + y \cdot C_p(\mathrm{Pu}O_2), \tag{48}$$

where y is the weight fraction of PuO_2.

Effect of Porosity on Thermal Conductivity

Attempts to evaluate the decrease in thermal conductivity due to porosity (P) have been made by Eucken in as early as 1932. There are many relations in the

literature describing the effect of porosity on thermal conductivity. Some of them are listed below [1, 64, 97–106]:

1. Loeb	$\lambda_M = (1 - P)\,\lambda_{TD}$	(i)
2. Modfied Loeb	$\lambda_M = (1 - \alpha P)\,\lambda_{TD}$ where $2 < \alpha < 5$	(ii)
3. Kampf and Karsten	$\lambda_M = \left(1 - P^{2/3}\right)\lambda_{TD}$	(iii)
4. Biancharia	$\lambda_M = [(1 - P)/(1 - (\beta - 1)P)]\,\lambda_{TD}$ $\beta = 1.5$ for spherical pores	(iv)
5. Maxwell-Eucken	$\lambda_M = [(1 - P)/(1 + \beta P)]\,\lambda_{TD}$	(v)
6. Brand and Neuer	$\lambda_M = (1 - \sigma P)\,\lambda_{TD}$ where $\sigma = 2.6 - 0.5\ (T + 273)/1000$	(vi)
7. Schultz	$\lambda_M = (1 - P)^{\gamma}\,\lambda_{TD}$	(vii)

(λ_M and λ_{TD} are the thermal conductivities, respectively, in presence and absence of porosity P, $0 < P < 1$).

Schultz [106] has theoretically shown that, for spherical pores distributed randomly, γ of Eq. (vii) has a value of 1.5. However, in reality the above coefficients for fuel pellets are larger ($\gamma > 1.5$), due to the porosity being neither spherical nor uniformly distributed [1]. IAEA [40] has recommended the value of $\alpha = 2.5 \pm 1.5$ for the modified Loeb equation for $0 < P < 0.1$. Inoue, Abe, and Sato [107] experimentally showed that $\gamma = 2.4$ for $0.044 < P < 0.470$ and reported that $\beta = 2$ (Eq. (v)). The IAEA recommendation ($\alpha = 2.5 \pm 1.5$) is in agreement with other experimenters [1, 40]. Among the above, Eq. (i) under predicts the data and Eq. (iv) accounts for the shape of the pores.

5.2 Thermal Conductivity of ThO_2

The thermal conductivity of ThO_2 up to 1,800 K is reasonably well established (Table 12). Most of the data were derived from thermal diffusivity measurements. Peterson and Curtis [26] compiled data on thermal conductivity of ThO_2 to about 2,000 K. Bakker et al. [38] systematically evaluated the data of various authors. They analyzed the data of Pears [102], Rodriguez et al. [82], McEwan and Stoute [103], Belle et al. [104], Peterson et al. [105], Faucher et al. [108], Kingery et al. [109], McElroy et al. [110], ARF [111], Weilbacher [112] and DeBoskey [113].

Assessing the A and B parameters has the advantage that data sets that were determined in different temperature ranges can easily be compared and that data sets with extremely large or small A and B parameters can be rejected. On this basis, Bakker et al. [38] rejected many data and accepted only that data which shows a small variation between the A and B parameters. Hence data of Murabayashi [114], McElroy et al. [110], Koenig [115] and Springer et al. [57] are only used in their assessment. The A and B parameters were averaged, which yielded $A = 4.20 \times 10^{-4}$ mKW^{-1} and $B = 2.25 \times 10^{-4}$ mW^{-1} and these values can be used as the recommended values for 95 % dense ThO_2 in the temperature

Table 12 Thermal conductivity measurement for ThO_2

Author	Year	Remarks
Kingery et al. [109]	1954	373–1,273 K
ARF [111]	1957	93.3 % TD: 527–824 K
Peterson et al. [105]	1966	373–1,473 K
Belle et al. [104]	1967	393 K
Springer et al. [57]	1968	573–2,173 K
McElroy et al. [110]	1968	92.7 % TD: 200–1,400 K
McEwan and Stoute [103]	1969	95.0 % TD: 333 K
Murabayashi et al. [114]	1970	293 K
Faucher et al. [108]	1970	91.6 % TD: 1,900–2,600 K
Touloukian [61]	1970	Review paper
Weilbacher [112]	1972	97 % TD: 400–2,550 K
Rodriguez et al. [82]	1981	773–1,773 K
Srirama Murti and Mathews [124]	1991	92.0 % TD: 573–1,573 K
Bakker et al. [38]	1997	Review paper
Pillai and Raj [93]	2000	300–1,200 K
Jain et al. [126]	2006	373–1,773
Kutty et al. [84]	2008	298–1,500 K
Lu et al. [145]	2012	Modeling

range between 300 and 1,800 K. Hence, thermal conductivity of pure ThO_2 can be expressed as:

$$\lambda_{ThO_2}(W/mK) = \left(4.20 \times 10^{-4} + 2.25 \times 10^{-4}\, T\right)^{-1} \tag{49}$$

Belle and Berman [12] reported the following equation for the thermal conductivity of 100 % dense ThO_2 in the temperature range 298–2,950 K,

$$\lambda_{ThO_2}(W/mK) = \left(0.0213 + 1.597 \times 10^{-4}\, T\right)^{-1} \tag{50}$$

To evaluate the thermal conductivity beyond 2,950 K, Belle and Berman first obtained an expression for thermal diffusivity up to 2,950 K as

$$\alpha_{ThO_2}\left(m^2/s\right) = (-34191.1 + 561.28\, T)^{-1} \tag{51}$$

Assuming there is no discontinuity, Belle and Berman [12] extrapolated thermal diffusivity data values from 2,950 to 3,400 K. Their results along with others are shown in Fig. 12. The only high temperature data available is that of Weilbacher [112] which was fitted by a dashed line. The fitted data of Cozzo et al. [95] and Kutty et al. [84] represent the lowest and highest values in the low temperature range.

Figure 13 shows the calculated value of thermal conductivity for fully dense ThO_2 from ambient to 3,400 K. There is a sudden increase in conductivity at 2,950 K discontinuity, from 2.03 to 3.05 W/m·K, which represents the change in the heat capacity occurring at that point. The lowest thermal conductivity in the

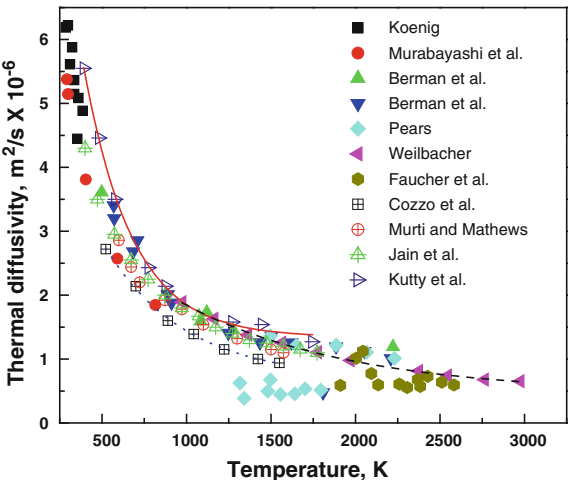

Fig. 12 Thermal diffusivity of ThO_2 as a function of temperature. Data of various authors are plotted together. Dotted line are fitted data of Cozzo et al. [95], dashed line that of Weilbacher [112] and solid line that of Kutty et al. [84]

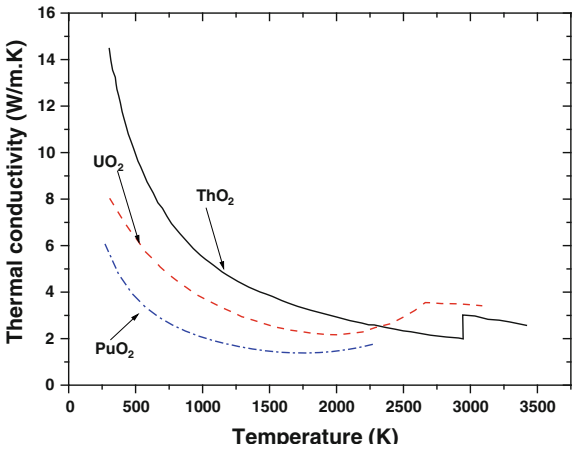

Fig. 13 Thermal conductivity of ThO_2, UO_2 and PuO_2 corrected for porosity and extrapolated to higher temperatures [6, 12, 40, 50]

entire temperature range was 2.03 W/m·K at 2,950 K. Belle and Berman [12] estimated minimum values in conductivity using Eq. (36). They assumed that:

1. Phonon velocity can be approximated to $(E/\rho)^{0.5}$,
2. Equation dealing temperature variation in E can be extrapolated to higher temperatures, and
3. Minimum value of phonon mean free path can be approximated to lattice parameter.

They calculated the minimum in thermal conductivity for ThO_2 at 2,950 K as 2.07 W/m·K which is very near to the value (2.03 W/m·K) shown in Fig 13. Thermal conductivity data of UO_2 [50] and PuO_2 [6, 40] are also shown in the same figure. The lowest value for UO_2 is 2.19 W/m·K at 1,970 K. The upswing in

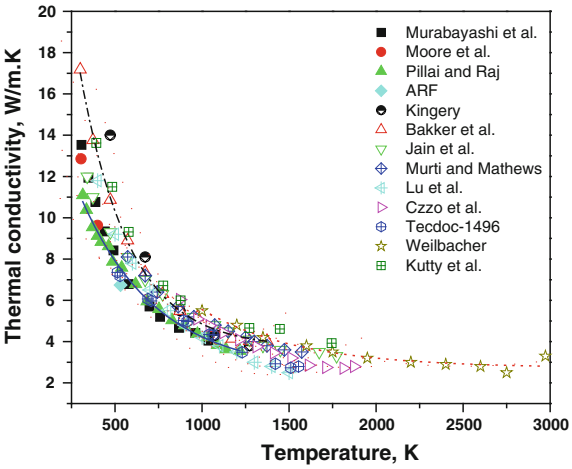

Fig. 14 Thermal conductivity of ThO_2 reported by various authors are corrected for 100 % density and plotted together. Solid line are fitted data of Pillai et al. [93], dotted line that of Weilbacher [112] and dashed line that of Bakker et al. [38]

thermal conductivity in UO_2 at $\sim$1,970 K can be explained in terms of the electronic contribution. On the other hand, increase in thermal conductivity beyond 2,950 K in ThO_2 is not result of electronic contribution, but is associated with increase in heat capacity. Thermal conductivity data of ThO_2 reported by various authors are shown in Fig. 14.

5.3 *Thermal Conductivity of UO_2*

There are many publications numbering over hundreds dealing with thermal conductivity of UO_2. Washington [116], Brandt and Neuer [117], and Fink et al. [50] made appraisals of the conductivity data found in the open literature. Brandt and Neur [117] presented a mean correlation curve of thermal conductivity versus temperature for UO_2 by using data from number of sources. Their equation had three terms: the first two terms are for phonon and electronic conductions, respectively. The third term stood for the decrease in thermal conductivity resulting from dislocations created at higher temperatures. Fink et al. [50] used a different model to fit the voluminous data on UO_2. They showed the evidence of a phase transition for UO_2 at 2,670 K from the enthalpy measurements and suggested a similar transition with temperature for thermal conductivity. Fink et al. [50] suggested a relation conforming with the enthalpy and heat capacity equations. Their relation is given below:

$$\lambda_{UO_2}(W.m-1.K-1) = \left(A + BT + CT^2\right)^{-1} + DTe^{-E/kT}, (298 \leq T \leq 2670\ K) \tag{52}$$

where $A = 6.8337 \times 10^{-2}$ m·K·W^{-1}, $B = 1.6693 \times 10^{-4}$ m·W^{-1}, $C = 3.1886 \times 10^{-8}$ m·W^{-1}K^{-1}, $D = 1.2783 \times 10^{-1}$ W·m^{-1} K^{-2}, $E = 1.1608$ eV, and k is the Boltzmann constant.

For 2,670 K $\leq T \leq$ 3,120 K,

$$\lambda_{UO_2}\left(W \cdot m^{-1} \cdot K^{-1}\right) = 4.1486 - 2.2673 \times 10^{-4}\, T \tag{53}$$

Equations (52) and (53) fit the thermal conductivity data within an error margin of 6.2 %. The two terms in Eq. (52) represent contributions from phonons and electrons, respectively. The inclusion of a dislocation term as recommended originally by Weilbacher [112] to fit his high temperature data was not justified.

In 2006, IAEA [40] made a detailed survey on thermal conductivity data and recommended equation for the thermal conductivity of 95 % dense solid UO_2 which consists of lattice term and a term suggested by Ronchi et al. [118] to represent the small-polaron ambipolar contribution to the thermal conductivity. The lattice term was determined by a least squares fit to the lattice contributions to the thermal conductivity obtained by Ronchi et al. [118], Hobson et al. [119], Bates [120], Conway et al. [121] and Godfrey et al. [122]. The recommended equation for thermal conductivity of solid 95 % dense UO_2 is:

$$\lambda_{UO_2} = \left[100/\left(7.5408 + 17.692t + 3.6142\,t^2\right)\right] + \left(6400/t^{2.5}\right) \exp(-16.35/t) \tag{54}$$

where, t is T/1,000, T is in K, and λ is the thermal conductivity in W·m^{-1} K^{-1}. Thermal conductivity values for 100 % dense UO_2 or for a different density may be calculated using the porosity relation derived by Brandt and Neurer [117], which is:

$$\lambda_0 = \lambda_p/(1 - \sigma p), \tag{55}$$

where, $\sigma = 2.6$–$0.5t$. Here, t is T/1,000 where T is in K, p is the porosity fraction, λ_p is the thermal conductivity of UO_2 with porosity p, and λ_0 is the thermal conductivity of fully dense UO_2.

Uncertainties in thermal conductivity values for 298–2,000 K are 10 %. From 2,000 to 3,120 K, the uncertainty increased to 20 % because of the large discrepancies between measurements by different investigators [40]. Typical thermal conductivity of 95 % dense UO_2 as a function of temperature is given in Fig. 15.

The lattice term has traditionally been determined by fitting the low temperature thermal conductivity data because the lattice contribution dominates the thermal conductivity at low temperatures. Figure 16 shows the total thermal conductivity, the lattice contribution, and the ambipolar contribution as a function of temperature that have been calculated from the equation of Ronchi et al. [118], which is given below:

$$\lambda_{UO_2} = [100/(6.548 + 23.533t)] + \left(6,400/t^{2.5}\right) \exp(-16.35/t), \tag{56}$$

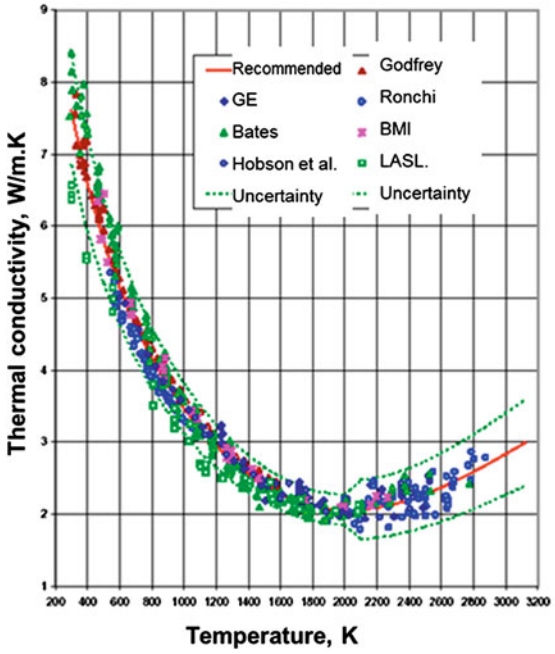

Fig. 15 Thermal conductivity data of 95 % dense UO_2 [40]. (permission from Elsevier)

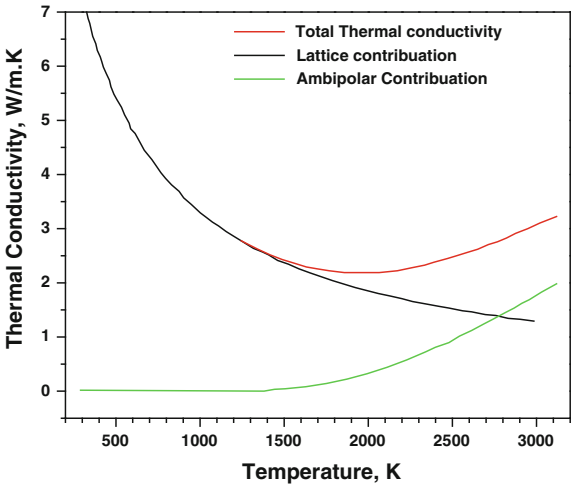

Fig. 16 Thermal conductivity of UO_2 showing lattice and electronic contributions [40]. (permission from IAEA)

where t is T/1,000, T is in K, and λ is the thermal conductivity for 95 % dense UO_2 in $W{\cdot}m^{-1}{\cdot}K^{-1}$. Below 1,300 K, the ambipolar term is insignificant and the total thermal conductivity equals the lattice contribution. Although the ambipolar term begins to have a significant contribution to the total thermal conductivity above

1,300 K, it is not larger than the lattice contribution determined by Ronchi et al. until 2,800 K. Even at 3,120 K, the lattice contribution is still significant.

No data is available on thermal conductivity of liquid ThO_2. Based on an initial review of the limited data [12, 40] on the thermal conductivity and thermal diffusivity of liquid UO_2, the liquid thermal conductivity is in the range of 2.5–3.6 $W \cdot m^{-1} K^{-1}$. Liquid thermal diffusivities range from 6×10^{-7} to 11×10^{-7} $m^2 s^{-1}$. The uncertainty in the thermal conductivity and thermal diffusivity of liquid UO_2 is approximately 40 % [40].

5.4 Thermal Conductivity of ThO_2–UO_2 Fuel

It is well known that the thermal conductivity of ThO_2 is higher than that of UO_2 by $\sim$50 % over a significant range of temperature. Berman et al. [123] made a systematic attempt to correlate thermal conductivity, temperature, and composition for ThO_2–UO_2 system in the early 1970s. Belle and Berman [12] updated the thermal conductivity correlation to 3,400 K by making use of the enthalpy data. Some information is available in literature for thoria—urania mixtures are from the work of Murti and Mathews [124], Lucuta et al. [125], Pillai et al. [93], Belle et al. [104], Kingery et al. [109], Berman et al. [123], IAEA-TECDOCs etc. (Table 13) but more data are still needed to completely characterize the thermal conductivity of (Th, U)O_2 fuel pellets. As a rule, in a homogeneous unirradiated mixture of ThO_2–UO_2, the thermal conductivity is somewhat higher than the thermal conductivity of unirradiated UO_2, depending on the temperature and the relative content of the ThO_2. However, it is worth mentioning that thermal conductivities of $(Th_{0.655}U_{0.345})O_2$ and $(Th_{0.355}U_{0.645})O_2$ pellets were found to be lower than that of both pure ThO_2 and UO_2 and degradation is large at low temperatures, but smaller as the temperature increases [67].

Mcelroy et al. [110] have measured the thermal conductivity of sol–gel-derived ThO_2 fuels from 80 to 1,400 K and compared with similar measurements on UO_2. Murabayakshi et al. [114] reported the thermal conductivity of ThO_2 pellets having densities ranging from 90 to 95 %. In respect of the porosity dependence of the thermal conductivity, the experimental results deviated significantly from the relationship derived by Loeb, and a modified Maxwell model was introduced to explain the data. Jain et al. [126] reported thermal diffusivity of a range of thoria–lanthana solid solutions in the compositional range from pure thoria to 10 mol% $LaO_{1.5}$ by the laser-flash method covering a temperature range from 373 to 1,773 K, and reported that thermal conductivity of thorium oxide–lanthanum oxide solid solutions decreases with increasing lanthanum content and temperature. Ronchi et al. [118] measured thermal conductivity of $(Th_{0.88}U_{0.12})O_2$ in the temperature range of 573–1,573 K. Ferro et al. [127] evaluated diffusivity of $(Th_{0.94}U_{0.06})O_2$ and $(Th_{0.90}U_{0.10})O_2$ from 650–2,700 K. Lemehov et al. [4] presented a model for the lattice thermal conductivity of pure and mixed oxides based on the Klemens-Callaways approach for the dielectric heat conductance modeling

Table 13 Thermal conductivity measurements for $(Th_{1-y}U_y)O_2$

Authors	Year	Temperature range, *K*	Composition, % UO_2	Remarks
Kingery [109]	1959	373–1,070	0, 10, 26, 31, 100	
DeBoskey [113]	1962	570–1,100	0, 8, 10	
Harbinson et al. [155]	1966	1,073–2,073	10, 100	
Moore et al. [156]	1967	293–423	4.7, 6.1, 6.3	
Belle et al. [104]	1967	393	0, 10, 20, 30, 50, 90, 100	
Springer et al. [57]	1968	573–2,173	3, 5, 7, 10, 13, 20, 25, 30, 100	
Ferro et al. [127]	1968	873–1,673	1, 4, 10	
McElroy et al. [110]	1969	303–393 K		
MacEwan et al. [103]	1969	333	0, 1, 3	
Jacob [128]	1969	573–2,123 K	3.1, 7.7, 10.0	
Murabayashi [114]	1970	293–1,073	1, 3, 5, 10	
Berman et al. [123]	1972	573–2,273	0, 2, 5.10, 20	
Ferro et al. [127]	1972	923–2,973	6, 10	
KWU [76]	1979	370–1,663 K	5	
Young [5]	1979	ThO_2	0	Modeling
Rodriguez et al. [82]	1981	773–1,773	0, 20, 100	
Bask et al. [130]	1989	800–2,100 K	2	
Murti et al. [124]	1991	573–1,573 K		ThO_2–$LaO_{1.5}$ solid solutions
Konings et al. [39]	1995	273–2,200 K	<30 %	Review paper
Bakker et al. [38]	1997	273–1,073 K	<20 %	Review paper
Pillai et al. [93]	2000	300–1,200 K	2	
INEEL [67]	2002	293–1,673 K	65, 35	
Ronchi et al. [24]	2003	573–1,573	12	
Jain et al. [126]	2006	373–1,773 K	ThO_2–$LaO_{1.5}$ (<10 mol%)	ThO_2-lanthana
IAEA –TECDOC [40]	2006	873–1,873 K	2, 4, 6, 10	
Kutty et al. [84]	2008	298–1,500	4, 10, 20	

and on some correlations between thermoelastic properties of solids. The thermal conductivity of ThO_2 and $Th_{0.98}U_{0.02}O_2$ was measured from 300 to 1,200 K by Pillai and Raj [93] and they showed that the decrease in thermal conductivity of $Th_{0.98}U_{0.02}O_2$ over that of ThO_2 is due to the enhanced phonon–lattice strain interaction in the oxide. Murti and Mathews [124] measured thermal conductivity on thorium–lanthanum mixed oxide solid solutions covering a temperature range from 573 to 1,573 K and a compositional range from 0 to 30 mol% $LaO_{1.5}$ and reported that thermal conductivity of the solid solutions were found to decrease with increase in lanthanum oxide content or temperature. Kutty et al. [84] measured thermal conductivity of ThO_2, ThO_2–4 % UO_2, ThO_2–10 % UO_2 and ThO_2–20 % UO_2 made by coated agglomerate pelletization (CAP) process and reported that thermal conductivity decreased with UO_2 content. A study carried out by

INEEL [67] shows that ThO_2 has a higher thermal conductivity than UO_2, but (Th, U)O_2 containing 65 or 35 wt% ThO_2 has similar in thermal conductivity of UO_2.

An assessment of thermal conductivity data of both irradiated and unirradiated ThO_2 and $Th_{1-y}U_yO_2$ solid solutions has been made by Berman et al. [123]. They analyzed data of Springer et al. [57], Jacobs [128], Matolich and Storhok [129] and Belle et al. [12]. Berman et al. [123] suggested complex behavior of the parameters A and B of Eq. (39) on variation of the uranium content which is inconsistent with theory and data on other ThO_2 or UO_2 compounds containing substitutions. The assessment by Bakker et al. [38] used only those data sets that contain pure ThO_2, which show a systematic decrease of the thermal conductivity on increasing UO_2 content (for UO_2 concentrations up to 20 %). Since good agreement exists between the variation of the A and B parameter on substitution as determined by Murabayashi [114] and the variation of A and B of comparable compounds as well as that predicted by theory, these parameters are used to obtain a recommended thermal conductivity for $Th_{1-y}U_yO_2$. The uranium concentration dependence of the thus obtained A and B parameters were fitted to obtain an equation that is valid for uranium concentration up to 10 % and a theoretical density of 95 %:

$$A = 4.195 \times 10^{-4} + 1.112 \cdot y - 4.499 \cdot y^2, \tag{57}$$

$$B = 2.248 \times 10^{-4} - 9.170 \times 10^{-4} \cdot y + 4.164 \times 10^{-3} \cdot y^2 \tag{58}$$

The recommended equation for $(Th_{1-y}U_y)\ O_2$ containing up to 10 % UO_2 is:

$$\begin{aligned} \lambda_{(Th-U)O_2} \ = \ & \Big[4.195 \cdot 10^{-4} + 1.112 \cdot y - 4.499 \cdot y^2 \\ & + \left(2.248 \cdot 10^{-4} - 9.170 \cdot 10^{-4} \cdot y + 4.164 \cdot 10^{-3} \cdot y^2\right) \cdot T\Big]^{-1} \end{aligned} \tag{59}$$

The above equation is valid in the temperature range 300–1,173 K. Figure 17 shows thermal conductivity of ThO_2–UO_2 for various UO_2 contents.

An elaborative study has been reported in IAEA-TECDOC [40] on ThO_2 containing 4, 6, 10, and 20 % of UO_2. The following are the recommended equations for the thermal conductivity (λ) as a function of temperature (T/K) which is valid from 873 to 1,873 K:

$$\lambda[Th_{0.96}U_{0.04}]O_2 = 1/(-0.04505 + 2.6241 \cdot 10^{-4} \cdot T) \tag{60}$$

$$\lambda[Th_{0.80}U_{0.20}]O_2 = 1/(0.02771 + 2.4695 \cdot 10^{-4} \cdot T) \tag{61}$$

Subsequently, best-fit equation for thermal conductivity of $(Th_{1-y}U_y)O_2$ of 95 % theoretical density as a function of composition (y in wt%) and temperature (T/K) has been derived, which is valid through 873–1,873 K.

$$\lambda(y,\ T) \ = \ 1/[-0.0464 + 0.0034 \cdot y + (2.5185 \cdot 10^{-4} + 1.0733 \cdot 10^{-7} \cdot y) \cdot T] \tag{62}$$

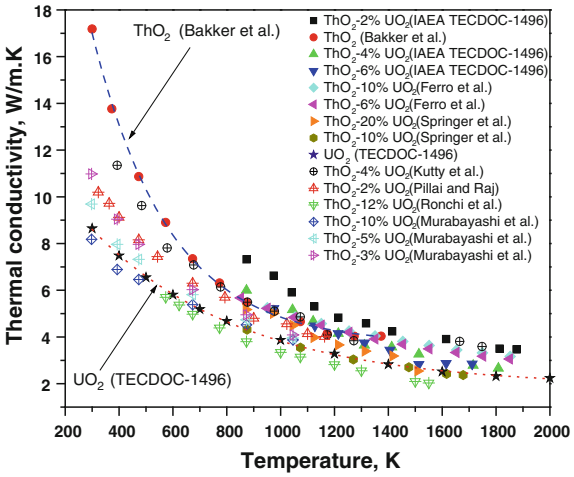

Fig. 17 Thermal conductivity of ThO_2-UO_2 fuels for various UO_2 contents reported in the literature. All the data used are corrected for 100 % density. Dashed line are fitted data of Bakker et al. [38] for pure ThO_2 and dotted line that of IAEA-TECDOC-1496 [40] for pure UO_2. (permission from IAEA)

5.5 *Thermal Conductivity of ThO_2–PuO_2 Fuel*

Although thoria-based fuels have been studied extensively in the past, namely in the 1970s, to our knowledge very little open literature is available for (Th, Pu)O_2 [40, 130]. Only a few measurements of thermal conductivity have been made for ThO_2–PuO_2 fuel. Since CeO_2 and PuO_2 have similar thermodynamic and crystallographic properties [131], Murbayashi [114] tried to simulate the thermal conductivity as a function of temperature and CeO_2 up to 10 wt% using Laser flash method. Jeffs [132, 133] determined the integral thermal conductivity of irradiated $(Th_{1-y}Pu_y)O_2$ containing 1.10, 1.75, and 2.72 wt% of PuO_2 using a steady state method. The thermal conductivity of a mixture of ThO_2 and 4 wt% PuO_2 was also measured by Basak et al. [130] using the laser flash technique for the temperature range of 950–1,800 K. Recently, Cozzo et al. [95] reported that at 500 K the thermal diffusivity of the Th-MOX can be down to 50 % of that of its pure oxide components ThO_2 and PuO_2. The presence of the two different oxides inside the Th-MOX lattice, generate a high amount of phonon scattering centers. When temperature increases, the plutonium concentration affects the thermal diffusivity of the fuel to a lesser extent, because the phonon–phonon scattering mechanism increases with temperature and becomes predominant when compared to the lattice strains due to the presence of either Th or Pu atoms in the lattice [95]. However, the thermal conductivity of pure PuO_2 was found to be higher than that of ThO_2 for all temperatures covered by their study. This is somewhat surprising and contradicts the understanding that ThO_2 always have a higher thermal conductivity than the other actinide oxides.

In Fig. 18, the thermal conductivity of Th-MOX with PuO_2 content varying from 0 to 30 wt% are shown. At low temperature, the thermal conductivity of the Th-MOX with a PuO_2 content from 0 to 30 wt% decreases with an increase of the

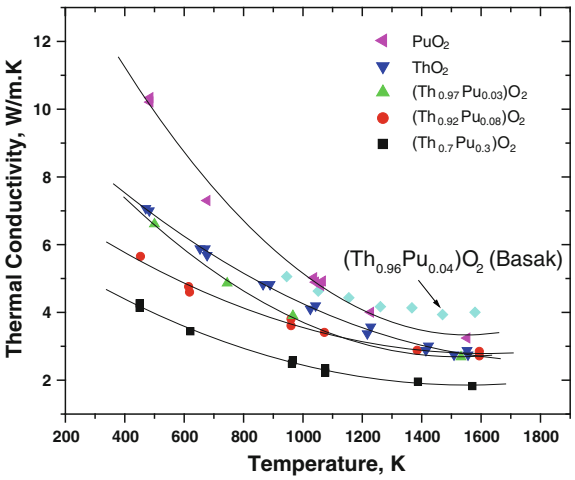

Fig. 18 Thermal conductivity of Th-MOX with PuO_2 content from 0 to 30 wt% [95]. (permission from Elsevier)

PuO_2 content. At higher temperature (above 1,000 K), the thermal conductivity of Th-MOX with a PuO_2 content from 0 to 8 wt% is almost independent from the concentration of plutonium. The conductivity of Th-MOX with 30 wt% PuO_2 at high temperatures is much lower [95].

The thermal conductivity λ, of $(Th_{1-y}Pu_y)O_2$ as a function of temperature and PuO_2 content is reported by IAEA study [40]. Figure 19 shows a systematic decrease of thermal conductivity with increasing PuO_2 content and temperature. The data are comparable with those obtained by Murabayashi [114] on simulated fuel samples of the composition ranging from 0 to 10 wt% CeO_2. The best-fit equation for the thermal conductivity, λ [W/m·K], of $(Th_{1-y}Pu_y)O_2$ as a function of composition, y [wt%], and temperature, T [K], was derived for the temperature range from 873 to 1,873 K [40].

$$\lambda(y,\ T)\ =\ 1/[-0.08388 + 1.7378 \cdot y + (2.62524 \cdot 10^{-4} + 1.7405 \cdot 10^{-4} \cdot y) \cdot T] \tag{63}$$

In order to introduce the influence of the plutonium content on parameter A, one can rely on the simplified theory of Abeles [95]. The parameter A has a second-order dependence on both the relative mass and radius differences as per the above theory. A polynomial equation of the second degree was chosen to define $A_{(PuO2)}$:

$$A_{(PuO_2)} = A_0 + A_1 \cdot [PuO_2] + A_2 \cdot [PuO_2]^2, \tag{64}$$

($[PuO_2]$ = Concentration of PuO_2 in wt%).

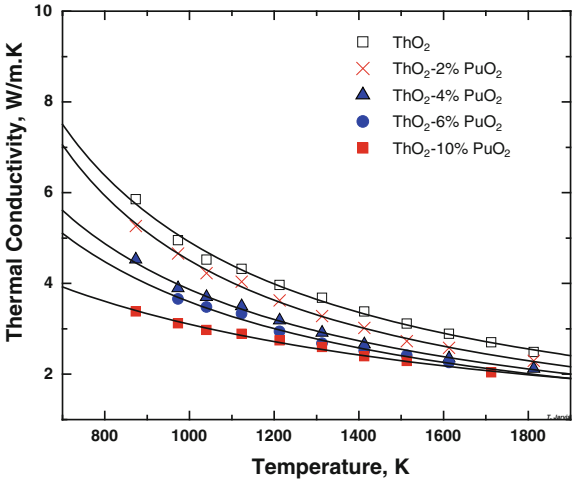

Fig. 19 Systematic decrease of thermal conductivity with increasing PuO_2 content and temperature for ThO_2–PuO_2 system [40]. (permission from IAEA)

The values of the parameters are [95]:

$$A_0 = 6.071 \times 10^{-3}\, mKW^{-1},$$
$$A_1 = 5.72 \times 10^{-1}\, mKW^{-1},$$
$$A_2 = -5.937 \times 10^{-1}\, mKW^{-1}.$$
$$B = 2.4 \times 10^{-4}\, mW^{-1}.$$

Figures 20 and 21 show the variation A and B parameters with PuO_2 content for ThO_2–PuO_2 system. The parameter A increases with increase in PuO_2 while the variation of B with PuO_2 content was found to be random.

The experimental thermal conductivity data of high Pu bearing hypostoichiometric and stoichiometric mixed thorium–plutonium oxide of compositions,

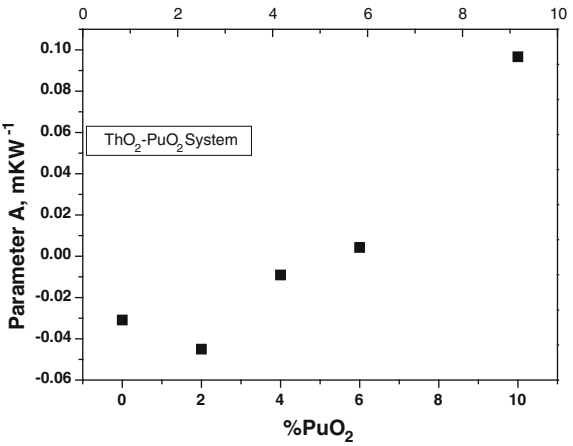

Fig. 20 Variation of parameter A with PuO_2 content

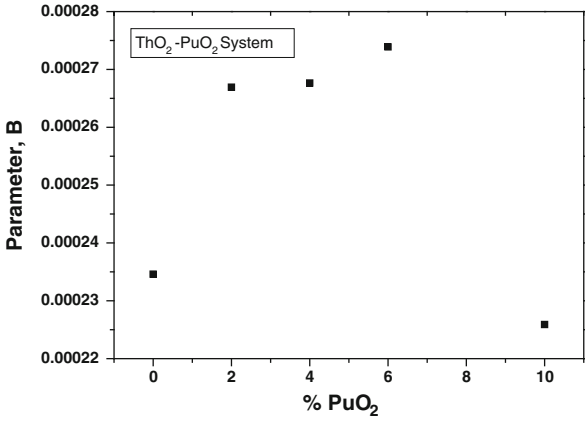

Fig. 21 Variation of the parameter B with PuO_2 content

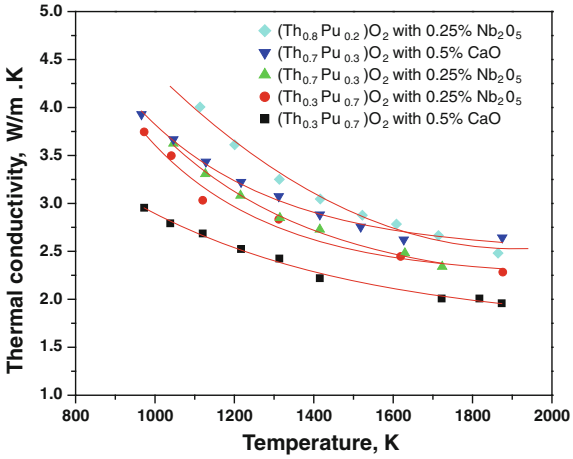

Fig. 22 Thermal conductivity data of ThO_2–20 % PuO_2, ThO_2–30 % PuO_2, and ThO_2–70 % PuO_2 with CaO or Nb_2O_5 as dopant [58]. (permission from IAEA)

ThO_2–20 % PuO_2, ThO_2–30 % PuO_2, and ThO_2–70 % PuO_2 with CaO or Nb_2O_5 as dopant, was measured up to 1,850 K in BARC, India, by employing the "Laser-flash" technique and is shown in Fig. 22. As expected, ThO_2–70 % PuO_2 showed the least thermal conductivity among the above sample.

6 Irradiation Behavior

Studies of irradiated fuels provide important data on the thermodynamics and chemistry of the fission products at high bumup. Generally, four distinct groups of fission products are observed in irradiated nuclear fuel [85, 125]:

(a) oxides dissolved in the matrix: Sr, Zr, Nb, Y, La, Ce, Pr, Nd, Pm, Sm;
(b) metallic precipitates: Mo, Tc, Ru, Rh, Pd, Ag, Cd, In, Sb, Te;
(c) oxide precipitates: Ba, Zr, Nb, Mo, (Rb, Cs, Te);
(d) gases and other volatile elements, e.g.: Kr, Xe, Br, I.

6.1 Studies on ThO_2

In India, ThO_2 has been extensively used in PHWRs for neutron flux flattening of the initial core during start-up. During the last few years, ThO_2 bundles have been utilized for this purpose in seven units of PHWR 220 including the two units each at Kakrapar Atomic Power Station (KAPS 1&2), Kaiga Atomic Power Station (KGS 1&2), Rajasthan Atomic Power Station (RAPS 3&4), and in RAPS 2 after mass coolant channel replacement. So far, some 232 thoria bundles have been successfully irradiated in the operating PHWR up to a maximum power of 408 kW and burnup of 13,000 MWd/Te HM without any failure [134]. Details of irradiation of ThO_2 bundles in India are shown in Table 14. In-pile irradiation of Zircaloy-clad (Th, Pu)O_2 fuel pins have been successfully carried out in the pressurized water loop of CIRUS research reactor. A six-pin cluster of free-standing Zircaloy–2 cladded ThO_2–4 % PuO_2 was successfully irradiated up to a burnup of 18,400 MWd/Te. Subsequently, two additional six pin clusters of collapsible Zircaloy–2 cladded pins containing high density ThO_2 and ThO_2–6.75 % PuO_2 were successfully irradiated up to a burnup of 10,300 MWd/Te without failure. The peak pin-power rating was 40 kW/m [135]. Details of ThO_2–PuO_2 pin irradiation are shown in Table 15.

Although several isolated irradiation experiments on ThO_2 and ThO_2–UO_2 materials have been conducted, the bulk of the irradiation data generated has come US from four goal-oriented programs [8, 12, 39, 136]:

1. Boiling water reactor (BWR) Program, which culminated in the irradiations performed in the BORAX-IV and Elk River reactors.
2. Thorium Utilization Program, which included the irradiation of vibratory compacted and pelletized fuels.

Table 14 Irradiation of ThO_2 bundles in Indian PHWRs

Reactor	Number of bundles
Madras-1	4
Kakrapar-I	35
Kakrapar-II	35
Rajasthan-II	18
Rajasthan-III	35
Rajasthan-IV	35
Kaiga-I	35
Kaiga-II	35

Table 15 Details of the irradiation of ThO_2–PuO_2 fuels

Fuel	Cladding type	Burnup (GWD/t)	Linear rating (kW/m)
ThO_2–4 % PuO_2	Free-standing	18.5	40
ThO_2–6.75 % PuO_2	Collapsible	10.2	42

3. Babcock and Wilcox developmental work on pressurized water reactor (PWR) fuels.
4. Light water breeder reactor (LWBR) Program at Bettis Atomic Laboratory which resulted in the core loading of the Shippingport Reactor.

The majority of experiments were performed on fuels with less than 10 wt% UO_2. From the above experiments and other experiments carried out in India, Russia, Canada, Japan, and Korea the following conclusions can be drawn about thermophysical properties.

6.2 Melting Point

The incorporation of transmuted elements into a solid phase is expected to change the melting point significantly. Because of the high melting points of urania and thoria, it would normally be expected that the introduction of other oxides would cause a decrease in the melting point [85]. No direct measurements were available on the effects of irradiation on melting points on ThO_2 or ThO_2–UO_2 solid solutions, but there are some data on UO_2 and simulated mixed oxide fuel. Christensen et al. [137] have measured the melting point of UO_2 and measured the effect of irradiation on melting point up to 13 fission units. They reported a nearly linear decrease of melting point of irradiated UO_2 with irradiation at a rate of 9 K per fission unit.[1] Konno et al. [138] studied melting temperature of simulated high burnup mixed oxide fuels for fast reactor corresponding to different burnup and found that melting temperature decreases with increase in fuel burnup. Yamamoto et al. [139] and Hirosawa et al. [140] also obtained similar results for FBR MOX fuel. Belle and Berman [12] derived that an irradiation of 1 fission unit (10^{26} fissions/m^3) should depress the melting point of thoria–urania fuel by about 5 K. This value differs from the 9 K per fission unit for urania may be due to a difference in the oxygen content or to the accumulation of about 0.3 mol% plutonia in the urania fuel [85].

[1] One fission unit = 4072 MWd/MTM (megawatt days per metric ton of heavy metal content) [85].

6.3 Thermal Conductivity

In general, the thermal conductivity is expected to decrease as a material is irradiated. This decrease is attributed to radiation damage to the lattice, and pellet cracking. The thermal conductivity measurements of irradiated and unirradiated materials can be approximately equal when the lattice damage is annealed during irradiation at high temperatures or thermal cycling as would occur during out-of-pile thermal conductivity measurements.

Effect of Irradiation on Conductivity

The thermal conductivity of irradiated nuclear fuel is affected by [12],

i. solid fission products—dissolved, and precipitated,
ii. pores and fission gas bubbles,
iii. deviation from stoichiometry,
iv. radiation damage, and
v. circumferential cracks.

The expression for the parametric dependence of irradiated fuel thermal conductivity, λ can be provided in a form of contributing factors for each individual effect [141–143]:

$$\lambda = k_I(\beta)\, x\, k_2(P)\, x\, k_3(x)\, x\, k_4(r)\, x\lambda_0(T)\ (W/mK), \tag{65}$$

where, $k_I(\beta)$ is the burnup (β) dependence factor, $k_2(P)$ is the porosity/bubbles (p) contribution, $k_3(x)$ describes the effect of O/M ratio (x-deviation from stoichiometry), $k_4(r)$ refers to the radiation damage, and λ_0 is the analytical expression for thermal conductivity of unirradiated fuel. Such an analytical expression can be easily adapted into fuel codes. The solid fission products formed during irradiation (dissolved and precipitated) affect the fuel thermal conductivity by changing the lattice contribution. Attempts have been made theoretically or experimentally to evaluate the effect of the fission products on thermal conductivity. It is shown that the dissolved fission products lower the thermal conductivity, whereas the precipitated fission products increase the thermal conductivity [5].

Radiation damage from neutrons, α-decay and fission increases the number of lattice defects and consequently reduces the thermal conductivity of the fuel. Early work at Chalk River showed that reactor radiation damage, for short irradiations, and below 1,000 K, results in a maximum reduction of about 25 % [8]. The decrease was very rapid at the beginning of the irradiation (10^{19}–10^{21} n/m^2, hence order of minutes to hours) and no further effect was found above about 10^{23} n/m^2. A limiting value of 3.5 W/m·K was reported for longer irradiations (up to 2.8×10^{24} n/m^2, corresponding to about a month of irradiation). Similar results were also obtained on irradiated ThO_2–1.3 wt% UO_2 in out-of-pile measurements [12].

Microstructural changes, lattice damage, fission depletion effects, and concomitant effect of pellet cracking leads to lowering thermal conductivity in irradiated fuels. The thermal resistivity relation developed by Belle and Burman

et al. [12] for oxide fuels can be modified by taking into the effects of irradiation by adding two terms to the resistivity of unirradiated material as:

$$R_{\text{irr}} = R_a + C/T + \text{DF}/T, \tag{66}$$

where, C and D are constants equal to 32.4 and 11.1, respectively. R_{irr} and R_a are in (m·K)/W, F is in fission units, and T is in K. The term C/T term accounts for the increase in thermal resistivity during the early stage of irradiation due to the lattice defects concentration caused by neutron and fission. The term DF/T account for the decrease in thermal conductivity, due to the accumulation of transmuted elements. These fission product atoms become more mobile with increasing temperature and tend to agglomerate and precipitate. A large number of reports on thermal conductivity of irradiated UO_2 fuel are available. It shows that below 773 K, thermal conductivity is reduced as a result of induced lattice defects. Between 773 K to melting point of UO_2, no substantial change in thermal conductivity is observed.

Jacobs [128] compared the unirradiated and in-pile-irradiated thermal conductivities of ThO_2–10 % UO_2. The data were fitted to equation and the thermal conductivity of the unirradiated specimen (λ_{un}) varied with temperature, T (°C), as shown in Equation:

$$\lambda_{\text{un}} = (8.4703 + 0.02551\,T)^{-1} \tag{67}$$

The thermal conductivity of the irradiated specimen (λ_{irr}) varied with temperature, T as

$$\lambda_{\text{irr}} = (10.5181 + 0.02003\,T)^{-1} \tag{68}$$

Jacobs [128] concluded that there is no statistical difference at the 0.99 confidence level between the thermal conductivity of unirradiated ThO_2–10 wt% UO_2 and ThO_2–10 wt% UO_2 irradiated to 0.26×10^{18} fissions/cm^3. MacEwan and Stoute [103] reported that thermal conductivity of ThO_2–1.3 mol% UO_2 at 333 K before and after irradiation and found that irradiation at low temperature decreased the thermal conductivity. Irradiation exposure varied from 3.1×10^{-6} to 4.7×10^{-4} fission units. Increasing the irradiation temperature to 600–629 K reduced the extent of decrease in thermal conductivity which may be due to the annealing of damage during irradiation. Thermal conductivity of ThO_2 and ThO_2–UO_2 compositions was measured by Jacobs [128] during the reactor irradiation and reported no statistically significant difference between in reactor and unirradiated values for ThO_2 and ThO_2–9.8 mol% UO_2 below 1,273 K. Matolich and Storhok [129] determined post-irradiation thermal conductivity of irradiated ThO_2–3 % UO_2, ThO_2–9.8 % UO_2, and ThO_2–14.8 % UO_2 (composition in mol%). They could not find any significant differences between irradiated and unirradiated measurements for ThO_2–3 % UO_2 which they concluded that due to the annealing of the lattice damages at high temperature irradiation at 1,173 K. For ThO_2–9.8 % UO_2, anomalous results were obtained but the results were uncertain. The measured post-irradiation conductivity of ThO_2–14.8 % UO_2 was lower. After annealing

between 573 and 1,473 K, irradiated thermal conductivities were about 55 % below the unirradiated values. But, the materials had internal cracks and annealing effect was improper. The above results point to the fact that no quantitative conclusions can be made regarding the lattice damage and fission depletion effects on the thermal conductivity of ThO_2 and ThO_2–UO_2.

The differences in properties will cause ThO_2–UO_2 fuel rods to behave somewhat differently than UO_2 fuel rods during both normal operation and design basis accident conditions. During normal operation, ThO_2–UO_2 fuel will operate with somewhat lower fuel temperatures and less fission gas release than UO_2 fuel at corresponding powers and burnups. Several important conclusions can be drawn from this analysis. The mixed ThO_2–UO_2 fuel, using a mixture of 70 wt% ThO_2 and 30 wt% UO_2, where the uranium is initially enriched to 19.5 wt% U-235, appears to have sufficient reactivity to be used for extended burnup cycles to 72 GWD/t in LWRs. Likewise, a mixture containing 35 wt% UO_2, with the same enrichment and 65 wt% ThO_2, appears suitable for extended cycles approaching 90 GWD/t of initial heavy metal. The in situ breeding of U-233 maintains a more uniform reactivity during the course of irradiation and reduces the need for burnable poisons [67].

6.4 Fission Gas Release Features

Fission gas release (FGR) is primarily dependent on fuel temperature and fuel burnup [58, 144]. Figure 23 show a plot of FGR versus element power. It compares fission gas behavior for both ThO_2 and UO_2. Below a linear rating of ~40 kW/m, fuel microstructure plays a minimal role in FGR due to the low fuel temperature. The Fig. 23 compares the performance between UO_2 and granular ThO_2 although non-granular thorium demonstrates superior performance. A granular ThO_2 results in elevated central temperatures (despite the higher thermal conductivity of the ThO_2), which subsequently causes increased fission gas release which is comparable to that of similarly operated UO_2 [3]. The granular fuel often contains networks of tunnels that assist fission gas transport to the free void volume. The ratio of the granular FGR to non-granular FGR above 40 kW/m is approximately 2–4. Therefore, high quality non-granular thorium fuel exhibits significantly less fission gas release (two to four times less), even at higher power ratings and burnups.

6.5 Dimensional Stability

Very little irradiation-induced swelling occurs in ThO_2–UO_2 fuels up to 4 at.% burnup. In general, the volume change is less than 1 % for each at.% burnup. This relationship holds up to 10 at.%.

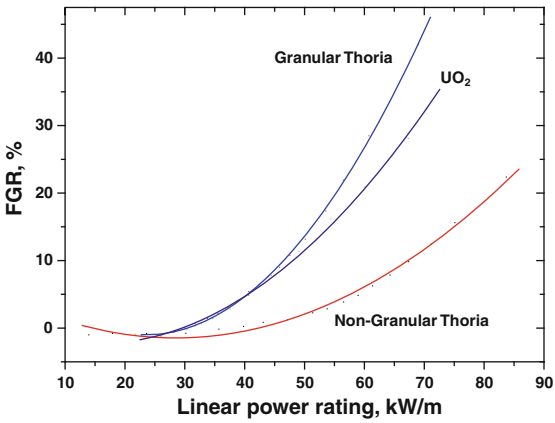

Fig. 23 Fission gas release from UO_2 and ThO_2 fuel [144]. (permission from IAEA)

6.6 Structural Stability

Post-irradiation examination (PIE) studies carried out on ThO_2 fuel bundles of KAPS irradiated up to 11,725 MWD/T of burnup showed excellent behavior of ThO_2 fuel during reactor operation. Gamma scanning was carried out on irradiated ThO_2 and UO_2 fuel pins of different burn-up to generate information on axial burnup distribution and power distribution profile in the fuel bundle using the ^{137}Cs as fission monitor. The relative power profile of UO_2 and ThO_2 fuel bundle showed significant difference. The inner ring fuel elements in ThO_2 fuel bundle showed higher power than the outer fuel elements in the bundle showing effect of epithermal neutrons. Figure 24 shows β–γ autoradiographs of the outer elements of UO_2 and ThO_2 having similar burn-up. Figure 24 shows that presence of Cs in cracks and also it can be noticed that number of cracks in ThO_2 is not as extensive like UO_2. The uniform presence of Cs in ThO_2 indicates that thermal gradients in ThO_2 are not large enough to cause migration of fission products [134].

6.7 ThO_2–PuO_2

PIE was carried out on experimental MOX (UO_2–4 % PuO_2) fuel elements of AC-4 cluster, that contained fuel elements pellets produced by different fabrication routes and varying pellet clad gaps and filler gas composition, after test irradiation in pressurized water loop (PWL) of CIRUS. Fuel pins with controlled porosity pellets and pellets with central hole showed very low fission gas release even at 110 W/cm^2 heat flux. Fuel pin containing low temperature sintered pellets showed abnormal gas release [134].

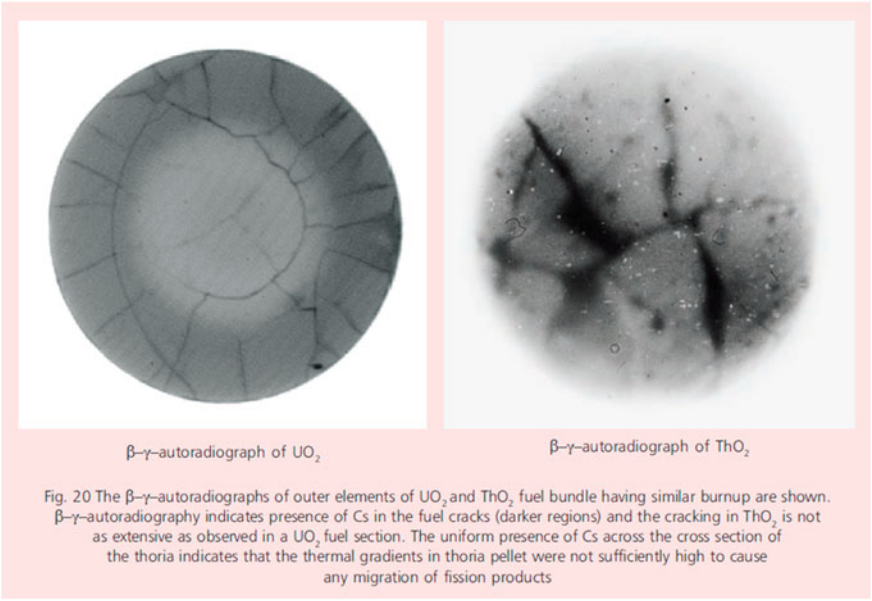

Fig. 24 *β–γ* autoradiographs of the outer elements of UO_2 and ThO_2 having similar burnup [134]

7 Conclusions

Improvement of the nuclear fuel exploitation has been one of the main objectives of reactor technology during the last decades. In recent years, considerable progress has been made in the understanding of fuel thermal performance. Accurate knowledge of the thermal properties of the fuel material is needed for assessment of reactor behavior under transient conditions. Assurances are needed that thermophysical properties available are sufficiently accurate and require further verification, documentation, peer review of existing data etc. Few selective measurements are also needed to obtain new data at conditions for which data are currently lacking or highly inadequate. There is also a need for international database and collaborative research on out-of-pile and in-pile property evaluation and irradiation testing especially on Th-based fuels.

Thermophysical data of ThO_2-based fuel, especially of ThO_2–PuO_2 system, are limited during irradiation and must be known prior to their use in existing or advanced reactors. Also high temperature properties of Th-based fuels at temperatures >2,000 K are very sparse and fresh attempts should be made to measure these data so that they can be effectively used by the fuel designers. A high confidence level on the fuel performance can only be reached from a good interpretation of the irradiation data followed by post-irradiation examinations. A prerequisite for this is to have data on out-of-pile properties such as thermal conductivity or thermal expansion that allows to understand the influence of

parameters such as temperature, temperature gradient, stress, stress gradient, fission rate, impurities that are effective during operation. Energy and matter transport processes were found to be strongly affected by reactor irradiation. Furthermore, in the severe reactor accidents, the fuel high temperature thermodynamic properties must comply with safety requirements to be satisfied under conditions which have been not yet explored.

Reports are available in the literature indicating that the irradiation performances of ThO_2–UO_2 fuel are superior over UO_2 fuels. However, data on cracking, swelling, microstructural changes, densification etc. for ThO_2–UO_2 and for ThO_2–PuO_2 fuels are needed to fully characterize these fuels during steady state operations. Also information on fission gas release to predict the internal pressurization, data on stored energy and fuel temperature distribution, knowledge on margin to fuel melting, propensity for rod failure during normal operating conditions are necessary. Knowledge on the comparative behavior for ThO_2–UO_2 to UO_2 fuel during reactivity insertion accidents, transient overpower operation, loss-of-coolant accidents, etc. are necessary for the licensing as well as for regulatory boards. In conclusion, a comprehensive data base for ThO_2–UO_2 and ThO_2–PuO_2 needs to be generated. A thorough understanding of thermophysical properties of the above systems is absolutely necessary to predict the behavior of fuels in a reactor.

Appendix 1

The coefficient of linear thermal expansion is defined as the differential change in length per unit change in temperature [32]. The instant temperature coefficient of the expansion is thus expressed as:

$$\alpha_l(T) = (1/L)\,(\delta L/\delta T)_P \tag{A1}$$

where, L is the length of the substance at temperature, T. The instant volume expansion coefficient, similarly defined, has the well-known connection to $\alpha_l(T)$ as $\alpha_V(T) \equiv (1/V)\ (\delta V/\delta T)_P = 3\alpha_l(T)$. The corresponding mean coefficient over a temperature interval (T_0 and T) is given by

$$\alpha_l = (1/L_0).(L - L_0)/(T - T_0) \equiv (1/\Delta T)(\Delta L/L_0), \tag{A2}$$

where, $\Delta T = T - T_0$ and $\Delta L = L - L_0$. Equation (A2) is more useful because most data compilations are given in terms of the dilation, $\Delta L/L_0$. For materials with isotropic thermal expansion property, the $\Delta L/L_0$ data can be directly correlated to the volume expansion and density lowering. This is so as the dilation factor (L/L_0) involved in Eq. (A2) can be used to express the corresponding volume ratio V/V_0 and equivalently, the density ratio (ρ_0/ρ) of the material as $V/V_0 \equiv \rho_0/\rho = (L/L_0)^3$, where $L/L_0 = 1 + \alpha_l\,\Delta T$. Like α_l one defines α_V, the mean volume expansion coefficient as $\alpha_V = (1/\Delta T)\,(\Delta V/V_0)$, which results in $V/V_0 = 1 + \alpha_V\,\Delta T$. Use of this result in the volume, or, density ratios leads to the

correlation between the two coefficients as $1 + \alpha_V\,\Delta T = (1 + \alpha_l\,\Delta T)^3$, which in other words leads to,

$$\alpha_v = 3\alpha_l + 3\alpha_1^2\Delta T + \alpha_1^3(\Delta T)^2 \tag{A.3}$$

The result reproduces the well-known correlation of instantaneous values of linear and volume expansion coefficients, $\alpha_V(T) = 3\alpha_l(T)$. The additional higher order terms involved in the correlation between the two mean coefficients generally making small contribution one can use the approximated form, $\alpha_v \approx 3\alpha_l$, for all practical purpose. The density ratio having the form,

$$\rho_0/\rho = (L/L_0)^3 \equiv (1 + \alpha_l\,\Delta T)^3, \tag{A.4}$$

can be approximated to $\rho_0/\rho \approx (1 + 3\alpha_1\,\Delta T)$, or equivalently, to $\rho_0/\rho \approx (1 + 3\Delta L/L_0)$. Thus, the fractional density change $(\rho_0 - \rho)/\rho_0 \equiv \Delta\rho/\rho_0$, is written as

$$\Delta\rho/\rho_0 \approx 3(\Delta L/L_0) \equiv 3\alpha_l\Delta T \tag{A.5}$$

The original relation $\rho_0/\rho = (L/L_0)^3$ can be approximated as

$$(L - L_0)/L_0 \equiv (\Delta L/L_0) \approx (\rho_0/\rho)^{0.33} - 1 \tag{A.6}$$

for expressing thermal dilations from tabulated values of density at different temperatures.

References

1. Olander DR (1976) Fundamental aspects of nuclear reactor fuel elements. TID-26711-P1, Energy Research and Development Administration, Oak Ridge
2. Matzke H (1986) Science of advanced LMFBR fuels: a monograph on solid state physics, chemistry and technology of carbides, nitrides and carbonitrides of uranium and plutonium. North Holland, Amsterdam
3. Olander DR (2009) Nuclear fuels—present and future. J Nucl Mater 389:1–22
4. Lemehov SV, Sobolev V, Van Uffelen P (2003) Modelling thermal conductivity and self-irradiation effects in mixed oxide fuels. J Nucl Mater 320:66–76
5. Young RA (1979) Model for the electronic contribution to the thermal and transport properties of ThO_2, UO_2, and PuO_2 in the solid and liquid phases. J Nucl Mater 87:283–296
6. Popov SG, Carbajo JJ, Ivanov VK, Yoder GL (2000) Thermophysical properties of MOX and UO_2 fuels including the effects of irradiation. Report ORNL/TM-2000/351, Oak Ridge National Laboratory, Oak Ridge
7. Kutty TRG, Ganguly C, Sastry DH (1995) Thermal expansion of Al-U and Al-U-Zr alloys. J Nucl Mater 226:197–205
8. Herring JS, MacDonald PE (1999) Characteristics of mixed thorium—uranium dioxide high burnup fuel. ANS annual meeting, June 6–10, Idaho National Engineering and Environmental Laboratory Report INEEL/CON-99-00141
9. Herring JS, MacDonald PE, Weaver KD, Kullberg C (2001) Low cost, proliferation resistant, uranium–thorium dioxide fuels for light water reactors. Nucl Eng Des 203:65–85

10. Oggianu SM, Kazimi MS (2000) A review of properties of advanced nuclear fuels. MIT report MIT-NFC-TR-021. Nucl Eng Dept MIT
11. Kazimi MS, Czerwinski KR, Driscoll MJ, Hejzlar PJ, Meyer JE (1999) On the use of thorium in light water reactors. MIT report MIT-NFC-TR-016. Nucl Eng Dept MIT
12. Belle J, Berman RM (1984) Thorium dioxide: properties and nuclear applications. Naval Reactors Office, United State Department of Energy, Government Printing Office, Washington
13. Olson GL, McCardell RK, Illum DB (1999) Fuel summary report: shippingport light water breeder reactor. Idaho National Engineering and Environmental Laboratory Report INEEL/EXT-98-00799 Rev.1
14. Lindemann FA (1910) The calculation of molecular vibration frequencies. Physik Z 11:609–612
15. Haire RG (1995) Comparison of the chemical and physical properties of f-element metals and oxides: their dependence on electronic properties. J Alloys Compd 223:185–196
16. Brooks MSS, Johansson B, Skriver HL (1984) Handbook on the physics and chemistry of the actinides, vol I. North-Holland, New York, pp 153–270
17. Yun Y, Oppeneer PM, Kim H, Park K (2009) Defect energetics and Xe diffusion in UO_2 and ThO_2. Acta Mater 57:1655–1659
18. Ruff O, Ebert F, Woitinek H (1929) Contribution to the ceramics of very refractory materials III: the system ZrO_2-ThO_2. Z Anorg Allgem Chem 180:252–256
19. Wartenberg H, Reusch HJ (1932) Schmelzdiagramme höchstfeuerfester oxyde. VI Berichtigung Z Anorg Allgem Chem 208:380–381
20. Geach GA, Harper ME (1953) Arc melting of non-metallic materials and a redetermination of the beryllia-thoria system. Metallurgia 47:269
21. Lambertson WA, Mueller MH, Gunzel FH (1953) Uranium oxide phase equilibrium systems: IV, UO_2–ThO_2. J Am Ceram Soc 36:397–399
22. Benz R (1969) Thorium-thorium dioxide phase equilibria. J Nucl Mater 29:43–49
23. Chikalle TD, McNeilly CE, Bates JL, Rasmussen JJ (1972) Collogues international C.N.R. S. No. 205, Etude Des transformations cristallines a haute temperature, Odeillo, 27–30 September, 1971
24. Ronchi C, Hiernaut JP (1996) Experimental measurement of pre-melting and melting of thorium dioxide. J Alloys Compd 240:179–185
25. Rand MH (1975) Thorium: physico-chemical properties of its compounds and alloys. Atom Energy Rev 5:35
26. Peterson S, Curtis CE (1970) Thorium ceramics data manual volume I—oxide. Report ORNL-4503 Oak Ridge Nation Laboratory, Oak Ridge
27. Christensen JA (1962) Irradiation effects on uranium dioxide melting. Report HW-69234, Hanford Atomic Product Division, Richland
28. Hohorst JK (ed) (1990) SCDAP/RELAP5/MOD2 code manual, vol 4: MATPRO a library for material properties for light water reactor accident analysis. NUREG/CR-5273
29. Brassfield HC, White JF, Sjodahl L, Bittel JT (1968) Recommended property and reactor kinetics data for use in evaluating a light water coolant reactor loss-of-coolant incident involving Zircaloy-4 or 304-SS-Clad UO_2. Report GEMP-482, General Electric Co Cincinnati, Ohio
30. Lyon WL, Baily WE (1967) The solid-liquid phase diagram for the UO_2-PuO_2 system. J Nucl Mater 22:332–339
31. Popov SG, Carbajo JJ, Ivanov VK, Yoder GL (2000) Thermophysical properties of MOX and UO_2 fuels including its effects of irradiation. ORNL/TM-2000/351, Oak Ridge National Laboratory, Oak Ridge
32. Rand MH, Ackermann RJ, Gronvold F, Oetting FL, Pattoret A (1978) Rev Int Des Hautes Temp et des Refract 15:355–365
33. Harding JH, Martin DG and Potter PE (1989) Thermophysical and thermochemical properties of fast reactor materials. Commission of European Communities Report EUR 12402

34. Latta RE, Fryxell RE et al (1970) Determination of solidus-liquidus temperatures in the UO_{2+x} system ($-0.50 < x < 0.20$). J Nucl Mater 35:195–210
35. Christensen JA (1964) Irradiation effects on uranium dioxide melting. United States Report HW-69234, Hanford Atomic Product Division, Richland
36. Ronchi C, Hiernaut JP, Selfslag R, Hyland GJ (1993) Laboratory measurement of the heat capacity of urania up to 8000 K: I. Experiment. Nucl Sci Eng 113:1–19
37. Christensen JA (1963) UO_2-ThO_2 phase studies. General Electric Report HW-76559, Richland, Washington
38. Bakker K, Cordfunke EHP, Konings RJM, Schram RPC (1997) Critical evaluation of the thermal properties of ThO_2 and $Th_{1-y}U_yO_2$ and a survey of the literature data on $Th_{1-y}Pu_yO_2$. J Nucl Mater 250:1–12
39. Konings RJM, Blankenvoorde PJAM, Cordfunke EHP, Bakker K (1995) Evaluation of thorium based nuclear fuels: chemical aspects. ECN-R-95-007, Netherlands Energy Research Foundation, ECN
40. IAEA-TECDOC 1496 (2006) Thermophysical properties database of materials for light water reactors and heavy water reactors. International Atomic Energy Agency, Vienna
41. Freshley MD, Mattys HM (1962) Ceramics research and development operation quarterly report October–December 1962. Report HW-76300. Hanford Power Products Division, Richland, Washington
42. Freshley MD, Mattys HM (1963) Properties of sintered ThO_2–PuO_2. Report HW-76302. Hanford Power Products Division, Richland, Washington
43. Gmelin Handbook der Anorgnischen Chemie (1978) Thorium, Suppl, vols C1 and C2 8th edn. Springer, Berlin
44. Mulford RNR, Ellinger FH (1958) ThO_2–PuO_2 and CeO_2–PuO_2 solid solutions. J Phys Chem 62:1466–1467
45. Dawson JK (1952) Magnetochemistry of the heaviest elements. Part VI. PuO_2–ThO_2 and PuF_4–ThF_4 solid solutions. J Chem Soc 1882–1886
46. Gronvold F (1955) High temperature X-Ray study of uranium oxides in UO_2–U_3O_8 region. J Inorg Nucl Chem 1:357–370
47. Martin DG (1988) The thermal expansion of solid UO_2 and (U, Pu) mixed oxides: a review and recommendations. J Nucl Mater 152:94–101
48. Harding JH, Martin DG, Potter PE (1989) Thermophysical and thermochemical properties of fast reactor materials. Commission of European Communities Report EUR 12402
49. Hutchings MT (1987) High-temperature studies of UO_2 and ThO_2 using neutron scattering techniques. J Chem Soc Faraday Trans II 83:1083–1103
50. Fink JK, Chasanov MG, Leibowitz L (1981) Thermophysical properties of uranium dioxide. J Nucl Mater 102:17–25
51. Benedict M, Pigford T, Levi HW (1981) Nuclear chemical engineering. McGraw-Hill
52. Cohen I, Berman RM (1966) A metallographic and X-ray study of the limits of oxygen solubility in the UO_2–ThO_2 system. J Nucl Mater 18:77–107
53. Olsen CS (1979) Fuel thermal expansion (FTHEXP). In: Hagraman DR, Reymann GA (ed) MATPRO- version 11: a handbook of materials properties for use in the analysis of light water reactor fuel rod behavior. US Nuclear Regulatory Commission Report NUREG/CR-0497
54. Momin AC, Venkateswarlu KS (1982) Thermophysical properties of ThO_2, UO_2 and mixed $(Th,U)O_2$. BARC report BARC-1171, Bhabha Atomic Research Centre, Trombay
55. Momin AC, Karkhanvala MD (1978) Temperature dependence of Gruneisen parameter and lattice vibrational frequencies of UO_2 and ThO_2 in the range 298-2300 K. High Temp Sci 10:45
56. Kempter CP, Elliott RO (1959) Thermal expansion of UN, UO_2, UO_2–ThO_2 and ThO_2. J Chem Phys 30:1524–1526
57. Springer JR, Eldridge EA, Goodyear MU, Wright TR, Lagerdrast JF (1967) Fabrication, characterization and thermal-property measurements of ThO_2–UO_2 fuel materials. Report No. BMI-X-10210, Battelle Memorial Institute Columbus

58. IAEA-TECDOC-1450 (2005) Thorium fuel cycle-Potential benefits and challenges. International Atomic Energy Agency, Vienna
59. Anthonysamy S, Panirselvam G, Vasudeva Rao PR (2000) In: Proceedings of the 12th national symposium on thermal analysis THERMANS 2000, Gorakhpur, p 29
60. Momin AC (1991) High temperature X-ray diffractometric studies on the lattice thermal expansion behaviour of UO_2, ThO_2 and $(U_{0.2}Th_{0.8})O_2$ doped with fission product oxides. J Nucl Mater 185:308–310
61. Touloukian YS, Kirby RK, Taylor RE, Lee LTYR (1970) Thermal expansion: nonmetallic solids. IFI/Plenum, New York
62. Breitung W, Reil KO (1990) The density and compressibility of liquid (U, Pu)-mixed oxide. Nucl Sci Eng 105:205–217
63. Dronting WD (1981) Thermal expansion of molten uranium dioxide. In: Proceedings of the 8th symposium on thermophysical properties. National Bureau of Standard, Gaithersburg, Maryland
64. Fink JK (2000) Thermophysical properties of uranium dioxide. J Nucl Mater 279:1–8
65. Christensen JA (1963) Thermal expansion and change in volume of uranium dioxide on melting. J Am Ceram Soc 46:607–608
66. Porter PE (2009) Over forty years of thermodynamics of nuclear materials. J Nucl Mater 489:29–44
67. MacDonald PE (2002) Advanced proliferation resistant, lower cost, uranium-thorium dioxide fuels for light water reactors. Idaho National Engineering and Environmental Laboratory Report INEEL/EXT-02-01411, Idaho
68. Shuller LC, Ewing RC, Becker U (2011) Thermodynamic properties of $Th_xU_{1-x}O_2$ $(0 < x < 1)$ based on quantum–mechanical calculations and Monte-Carlo simulations. J Nucl Mater 412:13–21
69. Yamashita T, Nitani N, Tsuji T, Inagaki H (1997) Thermal expansions of NpO_2 and some other actinide dioxides. J Nucl Mater 245:72–78
70. Goodman GL (1992) The electronic structure of actinide dioxides. J Alloys Compd 181:33–48
71. Taylor D (1984) Thermal expansion data: II. Binary oxides with the fluorite and rutile structures, MO_2, and the antifluorite structure, M_2O. Br Ceram Trans J 83:32–37
72. Hoch M, Momin AC (1969) High temperature thermal expansion of ThO_2 and UO_2. High Temp High Press 1:401–407
73. Ohnysty B, Rose FK (1964) Thermal expansion measurements on thoria and hafnia to 4500 °F. J Am Ceram Soc 47:398–400
74. Aronson S, Clayton JC (1960) Thermodynamic properties of non-stoichiometric Urania–Thoria solid solutions. J Chem Phys 32:749–754
75. Hirata K, Moriya K, Waseda Y (1977) High temperature thermal expansion of ThO_2, MgO and Y_2O_3 by X-ray diffraction. J Mater Sci 12:838–839
76. KFA, Nuclebras, KWU, NUKEM (1988) Program of research and development on the Thorium utilization in PWR's, final report (1979–1988). KFA, Jülich
77. Tyagi AK, Mathews MD (2000) Thermal expansion of ThO_2-2 wt% UO_2 by HT-XRD. J Nucl Mater 278:123–125
78. Anthonysamy S, Panneerselvam G, Bera Santanu, Narasimhan SV, Vasudeva Rao PR (2000) Studies on thermal expansion and XPS of thoria-urania solid solutions. J Nucl Mater 281:15–21
79. Springer JR, Eldrige EA, Goodyear MU, Wright TR, Langedrost JF (1967) Fabrication, characterization and thermal property measurements of ThO_2-UO_2 fuel materials. Battelle Memorial Institute Report BMI-X-10210, Columbus
80. Turner DN, Smith PD (1967) Linear thermal expansion of thoria, urania-thoria and their dispersion in beryllia in the range of 20–1000 °C together with the improved data of beryllia. Australian Atomic Energy Commission report AAEC E183, Lucas Heights
81. Lynch ED, Beals RJ (1962) Argonne national laboratory, annual report for 1962. ANL-6677, p 101

82. Rodriguez P, Sundaram CV (1981) Nuclear and materials aspects of the thorium fuel cycle. J Nucl Mater 100:227–249
83. Powers RM, Shapiro H (1959) Quarterly technical progress report. Sylvania Corning Nuclear Corporation, SCNC-301
84. Kutty TRG, Kulkarni RV, Sengupta P, Khan KB, Sengupta AK, Panakkal JP, Kamath HS (2008) Development of CAP process for fabrication of ThO_2-UO_2 fuels Part II: characterization and property evaluation. J Nucl Mater 373:309–318
85. Bhagat RK, Krishnan K, Kutty TRG, Kumar Arun, Kamath HS, Banerjee S (2012) Thermal expansion of simulated thoria–urania fuel by high temperature XRD. J Nucl Mater 422:152–157
86. Subramanian CGS, Panneerselvam G, Syamala KV, Antony MP (2009) Synthesis, characterization and thermal expansion studies on ThO_2–$SmO_{1.5}$ solid solutions. Ceram Int 35:2185–2190
87. Mathews MD, Ambekar BR, Tyagi AK (2006) Lattice thermal expansion studies of $Th_{1-x}Nd_xO_{2-x/2}$ solid solutions. Ceram Int 32:609–612
88. Grover V, Tyagi AK (2005) Lattice thermal expansion studies on single-phase compositions in CeO_2–ThO_2–ZrO_2 system. Ceram Int 31:769–772
89. Mathews MD, Ambekar BR, Tyagi AK (2001) Bulk thermal expansion studies of $Th_{1-x}Ce_xO_2$ in the complete solid solution range. J Nucl Mater 288:83–85
90. Kutty TRG, Khan KB, Hegde PV, Pandey VD, Sengupta AK, Majumdar S, Kamath HS (2002) Microstructure of ThO2–PuO2 pellets with varying PuO2 content. In: Ganguly C, Jayaraj PN (ed) Proceedings of CQCNF. Hyderabad, India
91. Fink JK, Petri MC (1997) Thermophysical properties of uranium dioxide. Argonne National Laboratory Report, ANL/RE-97/2
92. Klemens PG (1985) Theory of thermal conductivity of nonstoichiometric oxide and carbides. High Temp High Press 17:41–54
93. Pillai CGS, Raj P (2000) Thermal conductivity of ThO_2 and $Th_{0.98}U_{0.02}O_2$. J Nucl Mater 277:116–119
94. Degueldre C, Arima T, Lee YW (2003) Thermal conductivity of zirconia based inert matrix fuel: use and abuse of the formal models for testing new experimental data. J Nucl Mater 319:6–14
95. Cozzo C, Staicu D, Somers J, Fernandez A, Konings RJM (2011) Thermal diffusivity and conductivity of thorium–plutonium mixed oxides. J Nucl Mater 416:135–141
96. Clark LM, Taylor RE (1975) Radiation loss in the flash method for thermal diffusivity. J Appl Phys 46(2):714–719
97. Loeb AL (1954) Thermal conductivity VIII- a theory of thermal conductivity of porous materials. J Am Ceram Soc 37:96–99
98. Macewan JR, Stoute RL, Notley MF (1967) Effect of porosity on the thermal conductivity of UO_2. J Nucl Mater 24:109–112
99. Biancheria A (1966) The effect of porosity on thermal conductivity of ceramic bodies. Trans Am Nucl Soc 9:15
100. Ondracek G, Schultz B (1973) The porosity dependence of the thermal conductivity for nuclear fuels. J Nucl Mater 46:253–258
101. Vancraeynest JC, Stora JP (1970) Effect de la Porositesur la Variation de Conductubilite Thermique du Bioxyded'Uranium en Fonction de la Temperature. J Nucl Mater 37:153–158
102. Pears CD (1963) The thermal properties of twenty six solid materials to 5000 °F or their destruction temperatures. Report ASD-TR-62-765
103. MacEwan JR, Stoute RL (1969) Annealing of irradiation induced thermal conductivity changes in ThO_2-1.3 wt% UO_2. J Am Ceram Soc 52:160–165
104. Belle J, Berman RM, Bourgeois WF, Cohen I, Daniel RC (1967) Thermal conductivity of bulk oxide fuels. WAPD-TM-586, Bettis Atomic Power Laboratory, West Mifflin
105. Peterson S, Adams RE, Douglas DA (1966) Panel on utilization of thorium in power reactors. International Atomic Energy Agency Report STI/DOC/10/52, Vienna

106. Schultz B (1981) Thermal conductivity of porous and highly porous materials. High Temp High Press 37:649
107. Inoue M, Abe K, Sato I (2000) A method for determining an effective porosity correction factor for thermal conductivity in fast reactor uranium-plutonium oxide fuel pellets. J Nucl Mater 281:117–128
108. Faucher M, Cabannes F, Anthony AM, Piriou B, Simonato J (1970) Measurement of thermal diffusivity and total emissivity of solids between 1500 K and melting point. Rev Int Hautes Temp Refract 7:290–297
109. Kingery WD, Francl J, Cobble RL, Vasilos T (1954) Thermal conductivity data for several pure oxide materials corrected to zero porosity. J Am Ceram Soc 37:107–110
110. McElroy DL, Moore JP, Spindler PH (1968) Status and progress report for thorium fuel cycle development for 1967 and 1968. Oak Ridge National Laboratory Report ORNL-4429, pp 121–132
111. Armour Research Foundation (1957) ARF-Project No 6-025, final report
112. Weilbacher JC (1972) Measurement of the thermal diffusivity of mixed uranium plutonium oxides. High Temp High Press 4:431–438
113. DeBoskey WR (1962) Irradiation testing of thoria-urania fuel for the Indian point reactor. In: Proceedings of the Thorium fuel cycle symposium, TID-7650, Gatlinburg, TN, pp 630–642
114. Murabayashi M (1970) Thermal conductivity of ceramic solid solutions. J Nucl Sci Technol 7:559–563
115. Koenig JH (1953) Progress report no. 2 from March 1 to June 1, 1953. Rutgers Univ NJ Ceram. Research Sta AD-13154
116. Washington ABG (1973) Preferred values for the thermal conductivity of sintered ceramic fuel for fast reactor use. United Kingdom Atomic Energy Authority TRG-Report -2236
117. Brandt R, Neuer G (1976) Thermal conductivity and thermal radiation properties of UO_2. J Non-Equilib Thermodyn 1:3–23
118. Ronchi C, Sheindlin M, Musella M, Hyland GJ (1999) Thermal conductivity of uranium dioxide up to 2900 K from simultaneous measurement of the heat capacity and thermal diffusivity. J Appl Phys 85:776–789
119. Hobson IC, Taylor R, Ainscough JB (1974) Effect of porosity and stoichiometry on the thermal conductivity of uranium dioxide. J Phys D Appl Phys 7:1003–1015
120. Bates JL (1970) High-temperature thermal conductivity of round robin uranium dioxide. Battelle Memorial Institute Pacific Northwest Laboratories Report BNWL-1431
121. Conway JB, Feith AD (1969) An interim report on a round robin experimental program to measure the thermal conductivity of stoichiometric uranium dioxide. General Electric Report GEMP-715
122. Gofrey TG, Fulkerson W, Kollie TG, Moore JP, Mcelroy DL (1964) The thermal conductivity of uranium dioxide and armco iron by an improved radial heat flow technique. Oak Ridge national Laboratory Report ORNL-3556
123. Berman RM, Tully TS, Belle J, Goldberg I (1972) The thermal conductivity of polycrystalline thoria and thoria-urania solid solution. LMWR Development Program WAPD-TM-908
124. Murti PS, Mathews CK (1991) Thermal diffusivity and thermal conductivity studies on thorium-lanthanum mixed oxide solid solutions. J Phys D 24:2202–2209
125. Lucuta PG, Matzke H, Hastings IJ (1996) A Pragmatic approach to modeling thermal conductivity of irradiated UO_2 fuel: review and recommendations. J Nucl Mater 232:166–180
126. Jain D, Pillai CGS, Rao BS, Kulkarni RV, Ramdasan E, Sahoo KC (2006) Thermal diffusivity and thermal conductivity of thoria lanthana solid solutions up to 10 mol% $LaO_{1.5}$. J Nucl Mater 353:35–41
127. Ferro C, Patimo C, Piconi C (1972) Thermal diffusivity of mixed $(Th_{1-x}U_x)$oxides and some materials to be used as a reference in the range 650–2700 K. J Nucl Mater 43:273–276

128. Jacobs DC (1969) The in-pile thermal conductivity of selected ThO_2–UO_2 pellets at low depletions. Report WAPD-TM-758, Bettis Atomic Power Laboratory, West Mifflin
129. Matolich J, Storhok VW (1970) Thermal diffusivity measurements of irradiated oxide fuels. Battelle Memorial Institute Report BMI-RX-10274, Columbus
130. Basak U, Sengupta AK, Ganguly C (1989) Hot hardness and thermal conductivity of ThO_2–PuO_2 and ThO_2–UO_2 sintered pellets. J Mater Sci Lett 8:449–450
131. Altas Y, Tel H (2001) Structural and thermal investigations on cerium oxalate and derived oxide powders for the preparation of (Th, Ce)O2 pellets. J Nucl Mater 298:316–320
132. Jeffs AT, Boucher RR, Norlock LR (1967) Fabrication of UO_2–PuO_2 and ThO_2–PuO_2 experimental fuel. Report AECL-2675, Atomic Energy Canada Limited
133. Jeffs AT (1969) Thermal conductivity of ThO_2–PuO_2 under irradiation. AECL-3294, Atomic Energy of Canada Ltd, Chalk River
134. Anantharaman S, Ramadasan E, Singh JL, Dubey JS, Mishra Prerna (2010) Post Irradiation examination of thermal reactor fuels. BARC Newsletter 315:76–91
135. BARC Highlights (2006) Nuclear fuel cycle, post irradiation examination on fuel. Bhabha Atomic Research Centre, Trombay, p 39
136. Akabori M, Shiba K (1986) Dimensional changes in irradiated (Th, U)O_2. J Nucl Sci Technol 23:594–601
137. Christensen JA, Allio RJ, Biancheria A (1964) Melting point of irradiated uranium oxide. Trans Am Nucl Soc 7:390–391
138. Konno K, Hirosawa T (1999) Melting temperature of simulated high-burnup mixed oxide fuels for fast reactors. J Nucl Sci Technol 36:596–604
139. Yamamoto K, Hirosawa T, Yoshikawa K, Morozumi K, Nomura S (1993) Melting temperature and thermal conductivity of irradiated mixed oxide fuel. J Nucl Mater 204:85–92
140. Hirosawa T, Sato I (2011) Burnup dependence of melting temperature of FBR mixed oxide fuels irradiated to high burnup. J Nucl Mater 418:207–214
141. Bailly Henri, Menessier Denise, Prunier Claude (1999) The nuclear fuel of pressurized water reactors and fast neutron reactors—design and behaviour. Lavoisier Publishing Inc. Paris, France, p 138
142. Hart PE, Griffin CW, Hsieh KA, Matthews RB, White GD (1979) ThO_2 based fuels-their properties, methods of fabrication and irradiation performance: a critical assessment of the state of technology and recommendations for future work. Pacific Northwest Laboratory Report PNL-3069, Richland, Washington
143. Lucuta PG, Verrall RA, Matzke H, Palmer BJ (1991) Microstructural features of SIMFUEL—simulated high burn-up UO_2 based nuclear fuel. J Nucl Mater 178:48–60
144. IAEA Nuclear Energy Series No NF-T-2.4 (2012) Role of thorium to supplement fuel cycles of future nuclear energy systems. IAEA, Vienna
145. Lu Y, Yang Y, Zhang P (2012) Thermodynamic properties and structural stability of thorium dioxide. J Phys Condens Matter 24:225801
146. Aitken EA, Evans SK (1968) A thermodynamic data program involving urania at high temperatures. General Electric Report GEAP-5672
147. Adamson MG, Aitken EA, Caputi RW (1985) Experimental and thermodynamic evaluation of the melting behavior of irradiated oxide fuels. J Nucl Mater 130:349–365
148. Hagrman DT (1995) MATPRO - A library of materials properties for Light Water Reactor accident Analysis. SCDAP/RELAP5/MOD 3.1/Code manual, Vol. 4. MATPRO, USNRC Report NUREG/CR-6150 (EGGG-2720)
149. Komatsu J, Tachibana T, Konashi K (1988) The melting temperature of irradiated oxide fuel. J Nucl Mater 154:38–44
150. Marples JAC (1976) Plutonium 1975 and other actinides. In: Blank H, Lindner R (ed) North-Holland, Amsterdam, p 353
151. Fahey JA, Turcotte RP, Chikalla TD (1974) Thermal expansion of actinide oxides. Inorg Nucl Chem Lett 10:459–465
152. Zachariasen WH (1948) Crystal radii of heavy elements. Phys Rev 73:1104–1105

153. Baldock PJ, Spindler WE, Baker TW (1966) The X-ray thermal expansion of near—stoichiometric UO_2. J Nucl Mater 18:305–313
154. Katz JJ, Morse LR, Seaborg GT (1986) The chemistry of the actinide elements. Katz JJ, Morse LR, Seaborg GT (eds) Chapman and Hall, New York, vol 2, Ch 14, p 1121
155. Harbinson EN, Walker RJ (1966) Thermal conductance of ThO_2–10%UO_2 under simulated operating conditions. Trans Am Nucl Soc 9:26–27
156. Moore JP, Graves RS, Kollie TG, McElroy DL (1967) Thermal conductivity measurements on solids between 20 and 150 °C using a comparative longitudinal apparatus: results on M_gO, BeO, ThO_2, $Th_xU_{1-x}0_{2+y}$, and Al-UO_2 cermets. Oak Ridge National Laboratory Report ORNL-4121, Oak Ridge

http://www.springer.com/978-1-4471-5588-1

Thoria-based Nuclear Fuels
Thermophysical and Thermodynamic Properties, Fabrication, Reprocessing, and Waste Management
Das, D.; Bharadwaj, S.R. (Eds.)
2013, XII, 418 p. 173 illus., Hardcover
ISBN: 978-1-4471-5588-1